Sialylation of EGFR by ST6GAL1 induces receptor activation and modulates trafficking dynamics

Received for publication, June 5, 2023, and in revised form, August 6, 2023 Published, Papers in Press, September 1, 2023,
https://doi.org/10.1016/j.jbc.2023.105217

Katherine E. Ankenbauer, Tejeshwar C. Rao, Alexa L. Mattheyses*, and Susan L. Bellis*

From the Department of Cell, Developmental and Integrative Biology, University of Alabama at Birmingham, Birmingham, Alabama, USA

Reviewed by members of the JBC Editorial Board. Edited by Robert Haltiwanger

Aberrant glycosylation is a hallmark of a cancer cell. One prevalent alteration is an enrichment in α2,6-linked sialylation of N-glycosylated proteins, a modification directed by the ST6GAL1 sialyltransferase. ST6GAL1 is upregulated in many malignancies including ovarian cancer. Prior studies have shown that the addition of α2,6 sialic acid to the epidermal growth factor receptor (EGFR) activates this receptor, although the mechanism was largely unknown. To investigate the role of ST6GAL1 in EGFR activation, ST6GAL1 was overexpressed in the OV4 ovarian cancer line, which lacks endogenous ST6GAL1, or knocked-down in the OVCAR-3 and OVCAR-5 ovarian cancer lines, which have robust ST6GAL1 expression. Cells with high expression of ST6GAL1 displayed increased activation of EGFR and its downstream signaling targets, AKT and NFκB. Using biochemical and microscopy approaches, including total internal reflection fluorescence microscopy, we determined that the α2,6 sialylation of EGFR promoted its dimerization and higher order oligomerization. Additionally, ST6GAL1 activity was found to modulate EGFR trafficking dynamics following EGF-induced receptor activation. Specifically, EGFR sialylation enhanced receptor recycling to the cell surface following activation while simultaneously inhibiting lysosomal degradation. 3D widefield deconvolution microscopy confirmed that in cells with high ST6GAL1 expression, EGFR exhibited greater colocalization with Rab11 recycling endosomes and reduced colocalization with LAMP1-positive lysosomes. Collectively, our findings highlight a novel mechanism by which α2,6 sialylation promotes EGFR signaling by facilitating receptor oligomerization and recycling.

The receptor tyrosine kinase epidermal growth factor receptor (EGFR) has been the subject of intensive research due to its key roles in normal and aberrant epithelial cell physiology (1). During development and under normal physiological conditions, EGFR promotes cell survival and proliferation, and also regulates cell differentiation (2). Alterations in EGFR signaling are prevalent in many epithelial malignancies. EGFR and its ligands are commonly overexpressed (OE) in tumors, and moreover, EGFR frequently acquires mutations that drive constitutive receptor activation. This, in turn, promotes cell proliferation, angiogenesis, metastasis, and chemoresistance (3, 4). As an example of a cancer-associated EGFR alteration, EGFRvIII, a truncated form of EGFR, has a mutated ectodomain that mediates ligand-independent receptor activation (5). Many other cancer types harbor EGFR variants with mutations in the intracellular domain that foster protein stability (6). An understanding of EGFR activation and signaling is crucial for the therapeutic targeting of this receptor in cancer treatment.

EGFR and associated downstream signaling pathways are complex, and regulation occurs at multiple molecular levels. Under basal conditions, EGFR predominantly exists as an auto-inhibited monomer at the plasma membrane. However, when stimulated with EGF, the auto-inhibitory tether releases, facilitating receptor homodimerization, subsequent autophosphorylation of the cytosolic tails, and activation of intracellular signaling cascades such as PI3K/AKT/mTOR, Ras/Raf/MEK/ERK, and NFκB (7–9). Following activation, EGFR is internalized and then trafficked to various subcellular compartments depending upon the context (7). For instance, EGFR can be ubiquitinated and shuttled to the lysosome, where it is degraded, or recycled back to the cell surface to promote further signaling. Where EGFR localizes following activation and internalization depends upon factors such as the type and concentration of EGFR ligands within the microenvironment (10, 11). The balance between EGFR degradation and recycling is a key mechanism controlling how much signal the cell receives.

Another important factor in EGFR regulation is its glycosylation state. EGFR is a highly N-glycosylated protein, containing 11 canonical N-glycosylation consensus sequences and 4 noncanonical sequences (12, 13). Evidence suggests that all 11 canonical sites and one noncanonical site are glycosylated (14). Previous studies have shown that the N-glycosylation of EGFR is pivotal for its structure and function. N-glycans influence EGFR conformation, ligand binding capabilities, and the orientation of the EGFR ectodomain relative to the plasma membrane (15, 16). Furthermore, N-glycosylation at a specific site (Asn-579) plays an essential role in maintaining the autoinhibitory tether present in EGFR monomers (17). Thus, the glycosylation of EGFR exerts another layer of regulation in EGFR signaling.

* For correspondence: Susan L. Bellis, bellis@uab.edu; Alexa L. Mattheyses, mattheyses@uab.edu.

ST6GAL1 activates EGFR and modulates receptor trafficking

EGFR is aberrantly glycosylated in cancer cells due to alterations in the expression and activity of various glycosyltransferases. One such glycosyltransferase is the ST6GAL1 sialyltransferase, which is upregulated in numerous malignancies including ovarian cancer (18–21). ST6GAL1 adds an α2,6-linked sialic acid to the terminus of N-glycans on select glycoproteins including EGFR (22–27). We and others have shown that the α2,6 sialylation of EGFR activates this receptor (22–25); however, inhibitory effects of sialylation have also been reported (26–29). Furthermore, our group determined that the ST6GAL1-mediated sialylation of EGFR promotes epithelial-to-mesenchymal transition (22), resistance to the tyrosine kinase inhibitor (TKI), gefitinib (23), and mechanotransduction (24). These results point to a seminal role for EGFR sialylation in cancer cell behavior; however, the molecular mechanisms by which α2,6 sialylation regulates EGFR dynamics and downstream signaling remain largely unknown. In the present study, we report that ST6GAL1-mediated sialylation activates EGFR in seven different cancer cell models including ovarian, pancreatic, and colon cancer cells. To interrogate the mechanism of receptor activation, ST6GAL1 was overexpressed (OE) in the OV4 ovarian cancer line, which lacks endogenous ST6GAL1, or knocked-down (KD) in OVCAR-3 and OVCAR-5 ovarian cancer cells, which have high levels of ST6GAL1. Results from these models suggest that α2,6 sialylation of EGFR facilitates receptor dimerization and higher order clustering, leading to increased receptor activation and downstream signaling through AKT and NFκB. Additionally, the sialylation of EGFR by ST6GAL1 promotes recycling of the receptor to the cell surface while preventing degradation. Taken together, these results highlight a novel glycosylation-dependent mechanism by which cancer cells hijack EGFR signaling to enhance tumor-promoting signaling pathways.

Results

Cells with high levels of ST6GAL1 exhibit greater EGF-dependent activation of EGFR

To investigate the effects of ST6GAL1-mediated sialylation on EGFR activity, we assessed EGFR activation in pancreatic, ovarian, and colon cancer cell lines in which ST6GAL1 expression was directly modulated. The pancreatic cancer cell lines, MiaPaCa-2, S2-LM7AA, and S2-013, as well as the ovarian cancer cell lines, OVCAR-3 and OVCAR-5, have substantial ST6GAL1 expression, typical of most cancer cells. Accordingly, ST6GAL1 expression was KD in these lines (Fig. 1*A*). As controls, cells were transduced with either a nontargeting shRNA sequence (shC) or an empty vector (EV) construct. Conversely, ST6GAL1 was OE in the OV4 ovarian, and SW48 colon cancer lines, which have unusually low levels of endogenous ST6GAL1 (Fig. 1*B*). EV cells served as the control. The cell lines were treated with 100 ng/ml EGF for 15 min and EGFR activation was monitored by immunoblotting for phosphorylated EGFR (p-EGFR, pY1068). All of the cell lines with ST6GAL1 KD had diminished EGF-induced EGFR activation relative to controls (Fig. 1*C*), whereas the OV4 and SW48 lines with ST6GAL1 OE had enhanced EGFR activation compared with EV cells (Fig. 1*D*). These data show that α2,6 sialylation consistently activates EGFR in a wide range of cancer cell models, despite differences in genetic backgrounds or organ site. Furthermore, α2,6 sialylation activates EGFR in the SW48 cell model, which reportedly has an EGFR mutation (G719S) that causes ligand-independent receptor activation (30).

ST6GAL1-mediated sialylation does not alter the overall expression of EGFR or capacity of EGFR to bind ligand

To elucidate the molecular pathways by which ST6GAL1 regulates EGFR activation, we performed mechanistic studies using the three ovarian cancer cell lines, OV4, OVCAR-3, and OVCAR-5. We first confirmed that the modulation of ST6GAL1 expression led to a concomitant change in surface α2,6 sialylation. Cells were stained with *Sambucus nigra* agglutinin (SNA), a lectin that binds specifically to α2,6 sialic acids, and analyzed by flow cytometry. OV4 OE cells had increased surface levels of α2,6 sialic acid compared to EV cells, while OVCAR-3 and OVCAR-5 KD cells had reduced α2,6 sialylation compared to shC controls (Fig. 2*A*). We then verified that EGFR was a direct target for α2,6 sialylation, as has been previously reported (22–27). To this end, α2,6 sialylated proteins were precipitated using SNA-agarose, and the precipitates were immunoblotted for EGFR. OV4 OE cells had higher levels of α2,6 sialylated EGFR, whereas OVCAR-3 and OVCAR-5 KD cells had decreased levels of α2,6 sialylated EGFR, relative to their respective controls (Fig. 2*B*). Immunoblots of whole cell lysates used as inputs for SNA precipitation showed that modulating ST6GAL1 expression did not alter EGFR protein expression (Fig. 2*B*). We also measured basal levels of EGFR on the cell surface by flow cytometry. Cells with differential expression of ST6GAL1 had comparable levels of surface EGFR (Fig. 2*C*). To determine if α2,6 sialylation of EGFR affected ligand binding, cells were incubated with EGF concentrations ranging from 0.39 nM to 200 nM and EGF binding was quantified by flow cytometry to create a ligand binding curve. No significant differences were detected in the capacity of sialylated EGFR to bind EGF (Fig. 2*D*).

Levels of α2,6 sialylation directly correlate with EGFR activation

To corroborate the sialylation-dependent activation of EGFR, we evaluated EGFR phosphorylation in cells with high or low levels of surface α2,6 sialylation. WT OVCAR-3 and OVCAR-5 cells were used for these experiments because they naturally possess a range of α2,6 sialylation levels. OV4 cells were not included because they lack detectable expression of endogenous ST6GAL1. We first optimized a flow cytometry protocol for intracellular staining of p-EGFR. OVCAR-3 and OVCAR-5 cells were treated with or without EGF for 10 min to activate EGFR, and then permeabilized cells were incubated with antibody against p-EGFR (pY1068). As expected, EGF treatment increased the levels of p-EGFR (Fig. 3*A*). Next, we costained cells with SNA and anti-p-EGFR. OVCAR-3 and OVCAR-5 cells were gated for the 10% of cells with the highest

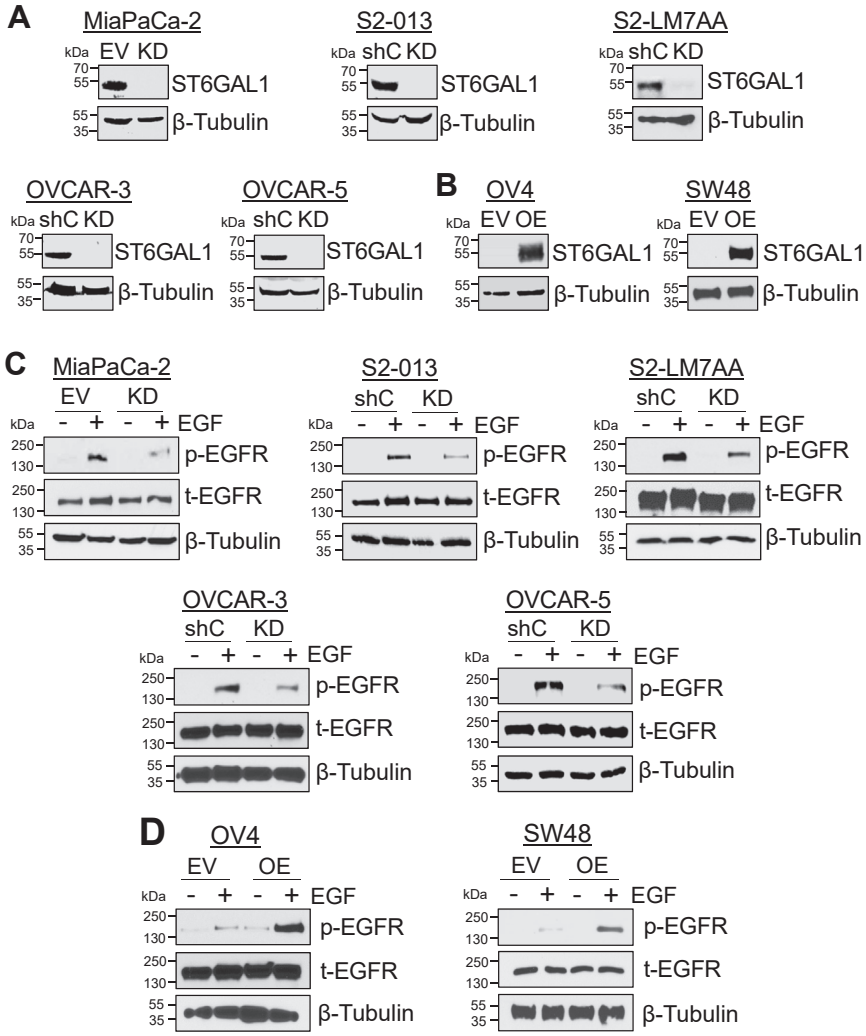

Figure 1. Sialylation of EGFR promotes its activation in multiple cell models. *A*, ST6GAL1 was stably knocked-down (KD) in cells with high endogenous ST6GAL1 expression (MiaPaCa-2, S2-013, S2-LM7AA, OVCAR-3, and OVCAR-5) using lentivirus encoding an shRNA sequence targeting ST6GAL1. As controls, cells were either transduced with lentivirus containing shRNA targeting GFP (shC) or with an empty vector (EV) construct. *B*, cells with undetectable endogenous ST6GAL1 (SW48 and OV4) were stably transduced with ST6GAL1-encoding cDNA to overexpress (OE) the enzyme, or with an EV construct. All cell lines represent polyclonal populations. *C*, cells were treated with 100 ng/ml EGF for 15 min and immunoblotted for p-EGFR (pY1068) and total EGFR (t-EGFR). *D*, cells treated with 100 ng/ml EGF for 15 min were immunoblotted for p-EGFR and t-EGFR. cDNA, complementary DNA; EGFR, epidermal growth factor receptor; p-EGFR, phosphorylated EGFR.

levels of surface α2,6 sialylation, and the 10% with the lowest levels of α2,6 sialylation, referred to as "SNA high" and "SNA low", respectively (schematic in Fig. 3*B*). The levels of p-EGFR in the SNA high and SNA low populations for OVCAR-3 (Fig. 3, *C* and *D*) and OVCAR-5 (Fig. 3, *E* and *F*) cells were quantified by obtaining the mean fluorescent intensity (MFI). Importantly, SNA high cells had significantly greater activation of EGFR as compared with SNA low cells both in the presence and absence of EGF treatment. These data indicate that high levels of ST6GAL1-mediated sialylation strongly correlate with an increase in EGFR activation.

Cells with high levels of ST6GAL1 display enhanced EGFR-mediated activation of AKT and NFκB p65, but not ERK

The activation of EGFR stimulates multiple downstream signaling molecules including AKT, NFκB, and ERK. To determine the effects of sialylation on EGFR signaling, OV4 cells were treated with EGF for 5, 15, and 30 min and evaluated for p-EGFR (pY1068). OE cells had higher levels of activated EGFR than EV cells (representative blot in Fig. 4*A*, quantification in Fig. 4*B*). Correspondingly, OE cells exhibited enhanced activation of AKT (Fig. 4, *C* and *D*) and NFκB p65 (Fig. 4, *E* and *F*). Intriguingly, no differences were noted in ERK activation in EV *versus* OE cells (Fig. 4, *G* and *H*).

Similar experiments were conducted with OVCAR-3 (Fig. 5) and OVCAR-5 (Fig. 6) cells with comparable results. In both cell models, ST6GAL1 KD decreased the activation of EGFR, AKT, and NFκB p65, but did not alter signaling by ERK. Of note, in OVCAR-5 cells, EGF treatment had little effect on ERK activation, which may relate to the fact that OVCAR-5 cells have a KRAS G12V mutation (31).

High ST6GAL1 expression promotes EGFR homodimer formation

We next assessed the formation of the EGFR homodimer, a critical step in the activation of EGFR and downstream

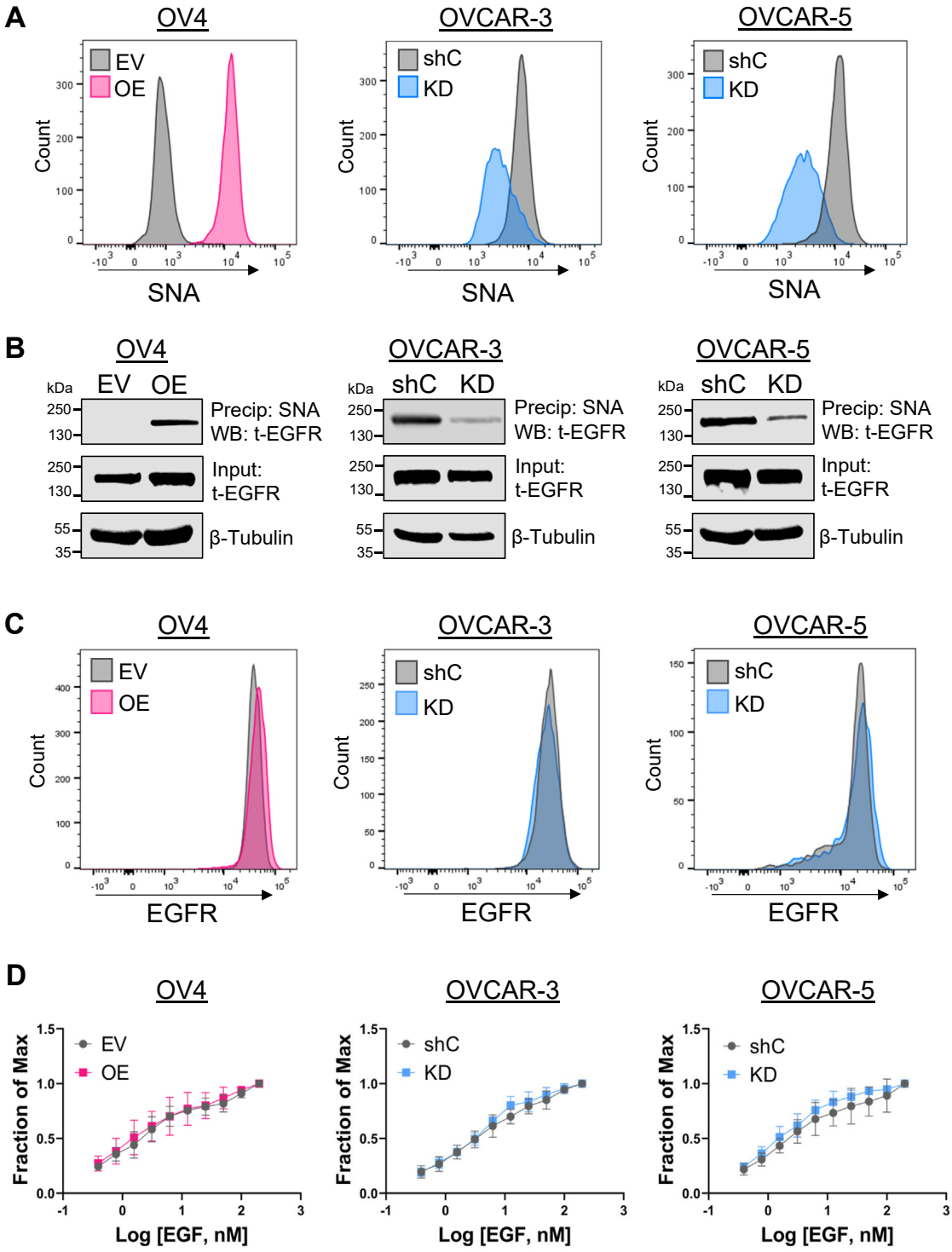

Figure 2. α2,6 sialylation of EGFR does not alter EGFR expression levels. *A*, levels of α2,6 sialylation on the cell surface were assessed by staining cells with SNA and measuring *via* flow cytometry. *B*, cell lysates were precipitated (Precip) with SNA-conjugated agarose and Western blotted (WB) for EGFR to determine the amount of α2,6 sialylated EGFR. Total EGFR expression was assessed by immunoblotting whole cell lysates (Input). *C*, cell surface EGFR expression was evaluated *via* flow cytometry. *D*, EGF binding was assessed using serial dilutions of EGF followed by flow cytometry. The *x*-axis depicts the log of the concentration of EGF and the *y*-axis is the fraction of maximal binding. Values are graphed as the mean ± S.D. EGFR, epidermal growth factor receptor; SNA, *Sambucus nigra* agglutinin.

signaling pathways (7). To monitor homodimerization, we adapted a protocol from Turk *et al*. 2015 (32), in which surface homodimers are stabilized using the bis[sulfosuccinimidyl] suberate (BS^3) cross-linking reagent. The presence of dimers on the cell surface was evaluated by immunoblotting, followed by densitometric quantification of the dimer to monomer ratio. In the OV4 cell line, significantly more dimer formation was observed in OE *versus* EV cells in the absence of EGF, as

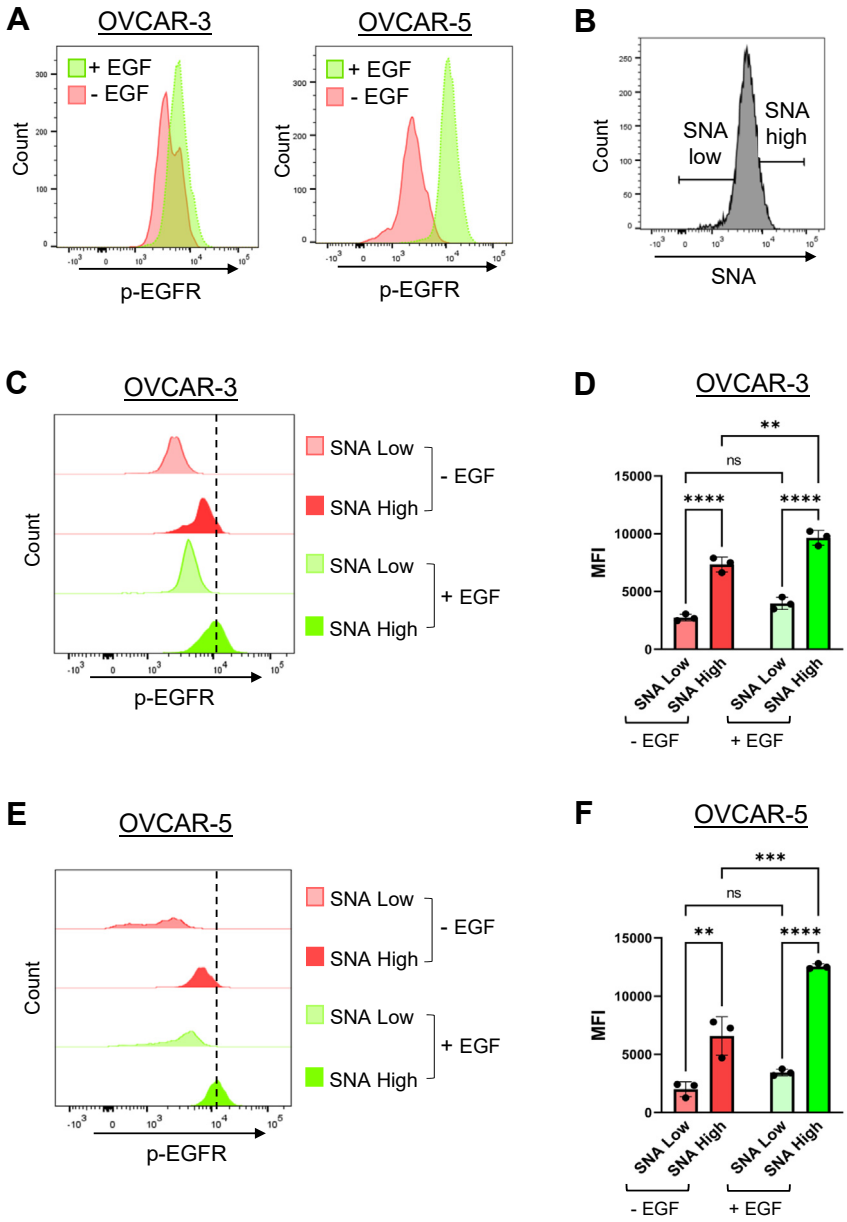

Figure 3. Cells with high levels of α2,6 sialylation have increased EGFR activation. OVCAR-3 and OVCAR-5 cells were treated with 100 ng/ml of EGF for 10 min, fixed, permeabilized, stained with SNA and/or p-EGFR, and then analyzed by flow cytometry. *A*, histograms depicting p-EGFR levels before and after treatment with EGF. *B*, schematic of the gating strategy for SNA staining. The 10% of cells with the lowest levels of α2,6 sialylation were designated as "SNA low", and the 10% of cells with the highest levels of α2,6 sialylation were designated as "SNA high". SNA high and SNA low cells were assessed for levels of p-EGFR. *C* and *D*, p-EGFR levels in OVCAR-3 SNA high and SNA low cells. Representative experiment in (*C*) and quantification in (*D*). *E* and *F*, p-EGFR levels in OVCAR-5 SNA high and SNA low cells. Representative experiment in (*E*); quantification in (*F*). *Dotted lines* indicate the highest peak of the histograms. Graphs depict the MFI ± S.D. from three independent experiments. (ns: $p > 0.05$, *$p < 0.05$, **$p < 0.01$, ***$p < 0.001$, ****$p < 0.0001$) as measured by a two-way ANOVA followed by Šidák's multiple comparison test. EGFR, epidermal growth factor receptor; MFI, mean fluorescent intensity; p-EGFR, phosphorylated EGFR; SNA, *Sambucus nigra* agglutinin.

well as following a 5-min EGF treatment (Fig. 7, *A* and *B*). In contrast, KD of ST6GAL1 in OVCAR-3 and OVCAR-5 cells led to a significant decrease in dimer formation, particularly at the early time points (Fig. 7, *C–F*).

Increased EGFR recycling is observed in cells with high levels of ST6GAL1

Following EGFR activation, EGFR internalizes into an early endosome, and then can either recycle back to the cell surface or translocate to the lysosome for degradation (7, 10). Accordingly, we evaluated the effects of ST6GAL1-mediated sialylation on EGFR recycling. Cells were first treated with cycloheximide (CHX) to prevent nascent EGFR synthesis (33). The levels of EGFR on the cell surface were then measured by flow cytometry for untreated cells, or cells treated with EGF for 15 min to stimulate EGFR internalization. As expected, EGF treatment induced EGFR internalization, as indicated by the leftward peak shift (these samples are labeled as "0 min recycling" in Fig. 8, *A*, *C*, and *E*). The amount of EGFR remaining on the cell surface following the 15-min EGF treatment was

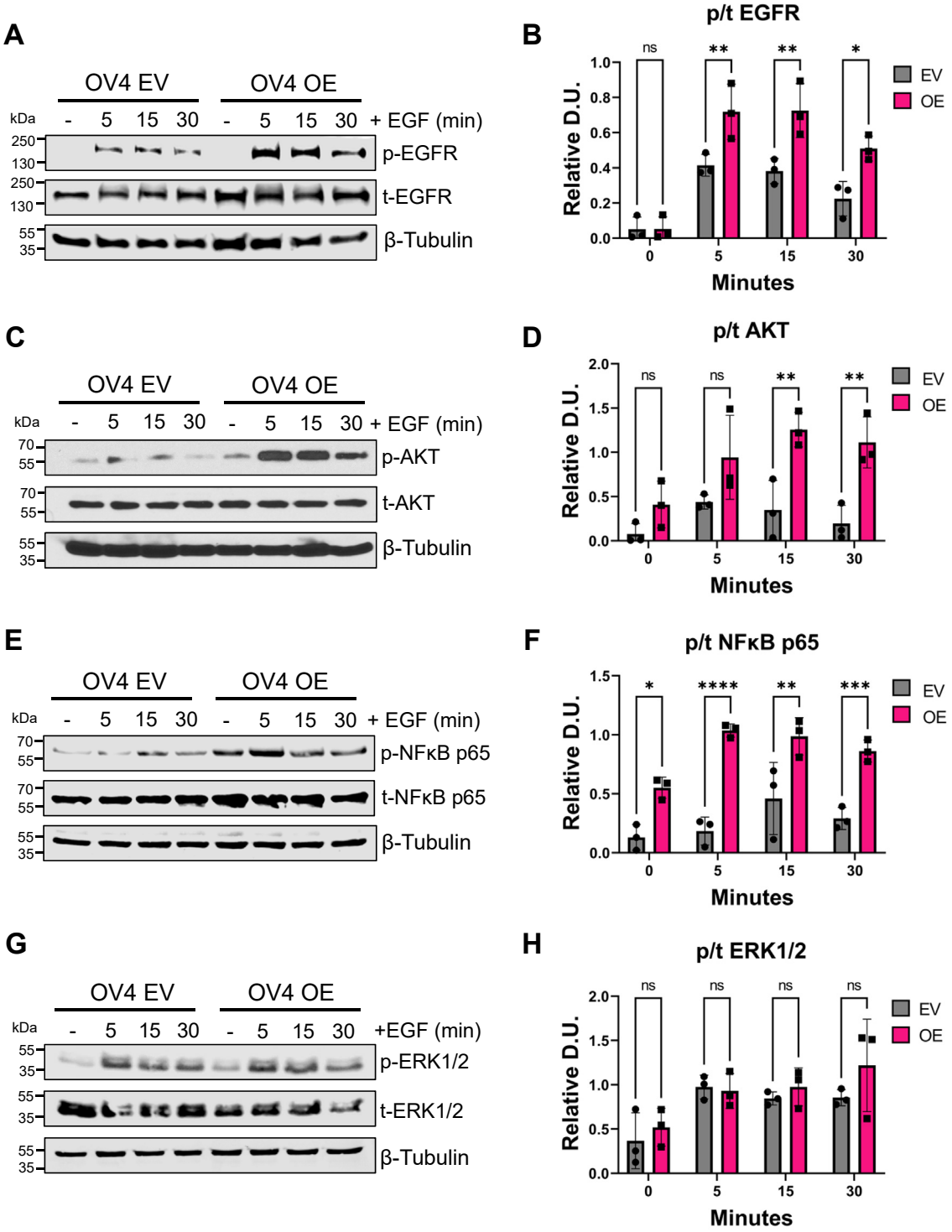

Figure 4. OV4 cells with ST6GAL1 overexpression have increased EGF-dependent activation of EGFR, AKT, and NFκB p65, but not ERK1/2. OV4 cells were treated with 100 ng/ml of EGF for 5, 15, or 30 min, or left untreated (–), and then cell lysates were immunoblotted for signaling molecules. *A* and *B*, representative blot (*A*) and quantification (*B*) of p-EGFR and t-EGFR. *C* and *D*, representative blot (*C*) and quantification (*D*) of p-AKT and t-AKT. *E* and *F*, representative blot (*E*) and quantification (*F*) of p-NFκB p65 and t-NFκB p65. *G* and *H*, representative blot (*G*) and quantification (*H*) of p-ERK1/2 and t-ERK1/2. Blots from three independent cell lysates were analyzed by densitometry and the phospho to total ratio (p/t) was calculated and normalized to β-tubulin. D.U. = densitometry units. Statistics were calculated using a two-way ANOVA followed by Šidák's multiple comparison test. (ns: $p > 0.05$, *$p < 0.05$, **$p < 0.01$, ***$p < 0.001$, ****$p < 0.0001$). EGFR, epidermal growth factor receptor; p-EGFR, phosphorylated EGFR; t-EGFR, total EGFR.

designated as time 0. The EGF-containing media was then replaced with EGF-free media and cells were incubated for an additional 60 min to allow EGFR recycling to the cell surface (samples labeled as "60 min recycling"). The percent recycling was calculated by comparing surface EGFR levels at the end of the 60-min recycling period with the levels of surface EGFR at

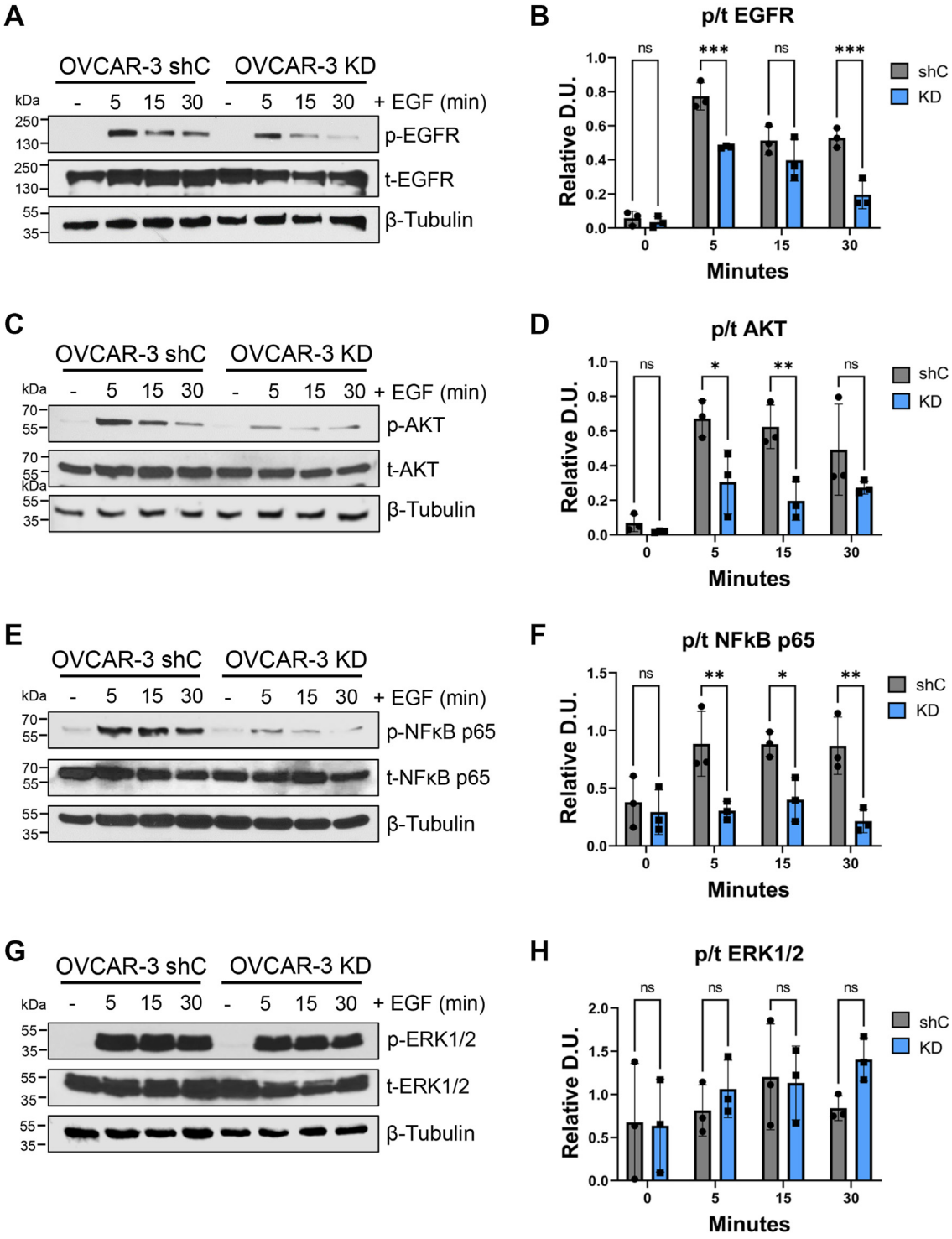

Figure 5. OVCAR-3 cells with ST6GAL1 knockdown have diminished EGF-dependent activation of EGFR, AKT, and NFκB p65, but not ERK1/2. OVCAR-3 cells were treated with 100 ng/ml of EGF for 5, 15, or 30 min or left untreated (–) and then cell lysates were immunoblotted for signaling molecules. *A* and *B*, p-EGFR and t-EGFR. *C* and *D*, p-AKT and t-AKT. *E* and *F*, p-NFκB p65 and t-NFκB p65. *G* and *H*, p-ERK1/2 and t-ERK1/2. The phospho to total ratio (p/t) was calculated and normalized to β-tubulin ("Relative D.U."). Graphs depict the mean ± S.D. for three independent immunoblots for each signaling molecule. Statistics were calculated using a two-way ANOVA followed by Šidák's multiple comparison test. (ns: $p > 0.05$, *$p < 0.05$, **$p < 0.01$, ***$p < 0.001$, ****$p < 0.0001$). EGFR, epidermal growth factor receptor; p-EGFR, phosphorylated EGFR; t-EGFR, total EGFR.

time 0. OV4 OE cells displayed significantly more EGFR recycling than EV cells (Fig. 8, *A* and *B*), whereas ST6GAL1 KD in OVCAR-3 and OVCAR-5 cells diminished EGFR recycling (Fig. 8, *C*–*F*).

ST6GAL1 activity protects EGFR from being degraded following EGF treatment

We next evaluated the effects of α2,6 sialylation on EGFR degradation following EGF treatment. Cells were pretreated

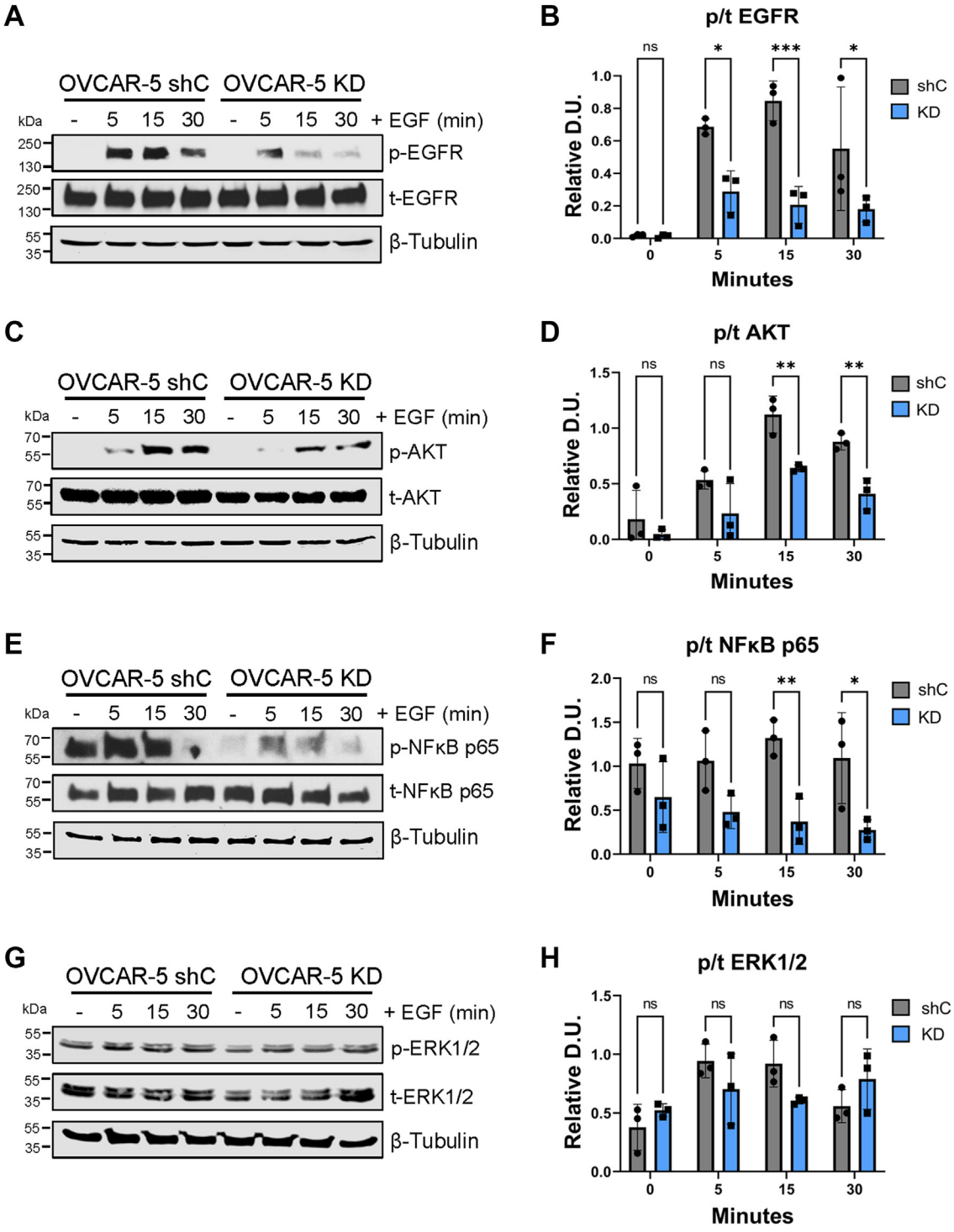

Figure 6. OVCAR-5 cells with ST6GAL1 knockdown have diminished EGF-dependent activation of EGFR, AKT, and NFκB p65, but not ERK1/2. OVCAR-5 cells were treated with 100 ng/ml of EGF for 5, 15, or 30 min or left untreated (–), and then cell lysates were immunoblotted for signaling molecules. *A* and *B*, p-EGFR and t-EGFR. *C* and *D*, p-AKT and t-AKT. *E* and *F*, p-NFκB p65 and t-NFκB p65. *G* and *H*, p-ERK1/2 and t-ERK1/2. The phospho to total ratio (p/t) was calculated and normalized to β-tubulin ("Relative D.U."). Graphs depict the mean ± S.D. for three independent immunoblots for each signaling molecule. Statistics were calculated using a two-way ANOVA followed by Šidák's multiple comparison test. (ns: $p > 0.05$, *$p < 0.05$, **$p < 0.01$, ***$p < 0.001$, ****$p < 0.0001$). EGFR, epidermal growth factor receptor; p-EGFR, phosphorylated EGFR; t-EGFR, total EGFR.

with CHX to prevent nascent EGFR synthesis and then incubated with EGF over a 120-min interval. As controls, cells were either left untreated, or treated for 120 min with CHX alone (to assess the amount of EGFR degradation in the absence of EGF). Notably, OV4 cells with ST6GAL1 OE exhibited minimal EGF-stimulated EGFR degradation over the 120-min incubation, while substantial degradation was observed in EV cells (Fig. 9, *A* and *B*). No differences were noted in the levels of EGFR in the absence of EGF treatment or in the presence of CHX alone, confirming that EGFR degradation was secondary

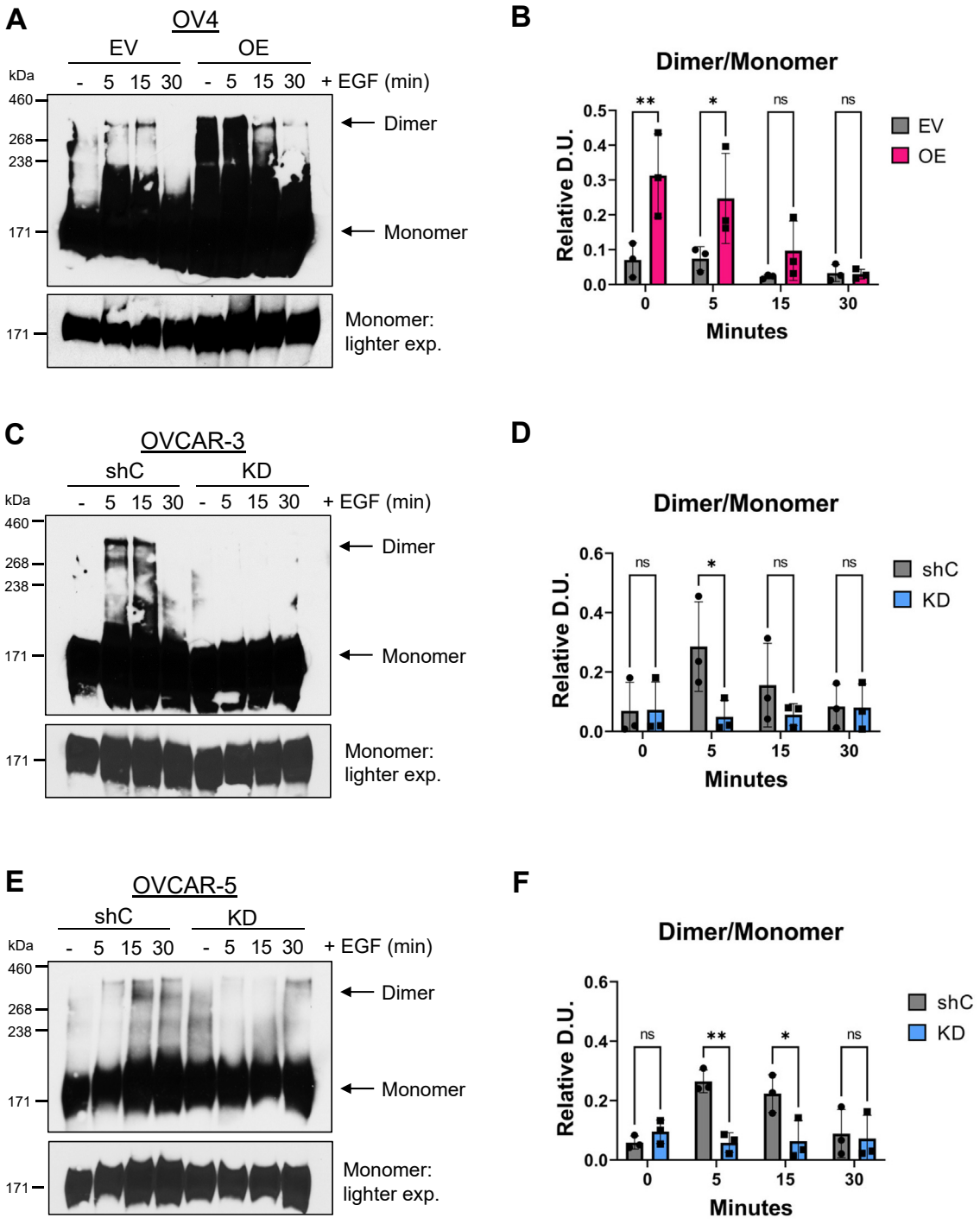

Figure 7. Cells with high ST6GAL1 expression have enhanced EGFR homodimer formation. Cells were treated with 100 ng/ml of EGF for 5, 15, or 30 min, or left untreated (–). After treatment, proteins were crosslinked using 3 mM of BS^3. Lysates were immunoblotted for EGFR. A high molecular weight ladder was used to distinguish monomers (~170 kDa) from dimers (~340 kDa). *A* and *B*, OV4 cells: representative immunoblot (*A*) and quantification (*B*) of the dimer to monomer ratio. A lighter exposure of the monomers (*lower panel* in *A*) was used for densitometric analyses. *B* and *C*, OVCAR-3 cells: representative immunoblot (*A*) and quantification (*B*) of the dimer to monomer ratio. *D* and *E*, OVCAR-5 cells: representative blot (*D*) and quantification (*E*) of the dimer to monomer ratio. Blots were analyzed by densitometry and the dimer to monomer ratio was calculated. Graphs depict mean ± S.D. from three independent experiments. Statistics were calculated using a two-way ANOVA followed by Šidák's multiple comparison test. (ns: $p > 0.05$, *$p < 0.05$, **$p < 0.01$). EGFR, epidermal growth factor receptor.

to the effects of EGF stimulation. Consistent with results from OV4 cells, OVCAR-3 and OVCAR-5 cells with ST6GAL1 KD exhibited more rapid EGFR degradation than shC cells (Fig. 9, *C–F*). These results suggest that α2,6 sialylation of EGFR protects against degradation following EGFR activation.

High expression of ST6GAL1 promotes higher-order EGFR clustering

To reinforce the biochemical assays described above, we evaluated EGFR activation and trafficking by microscopy. We utilized the OV4 cell model for these studies because

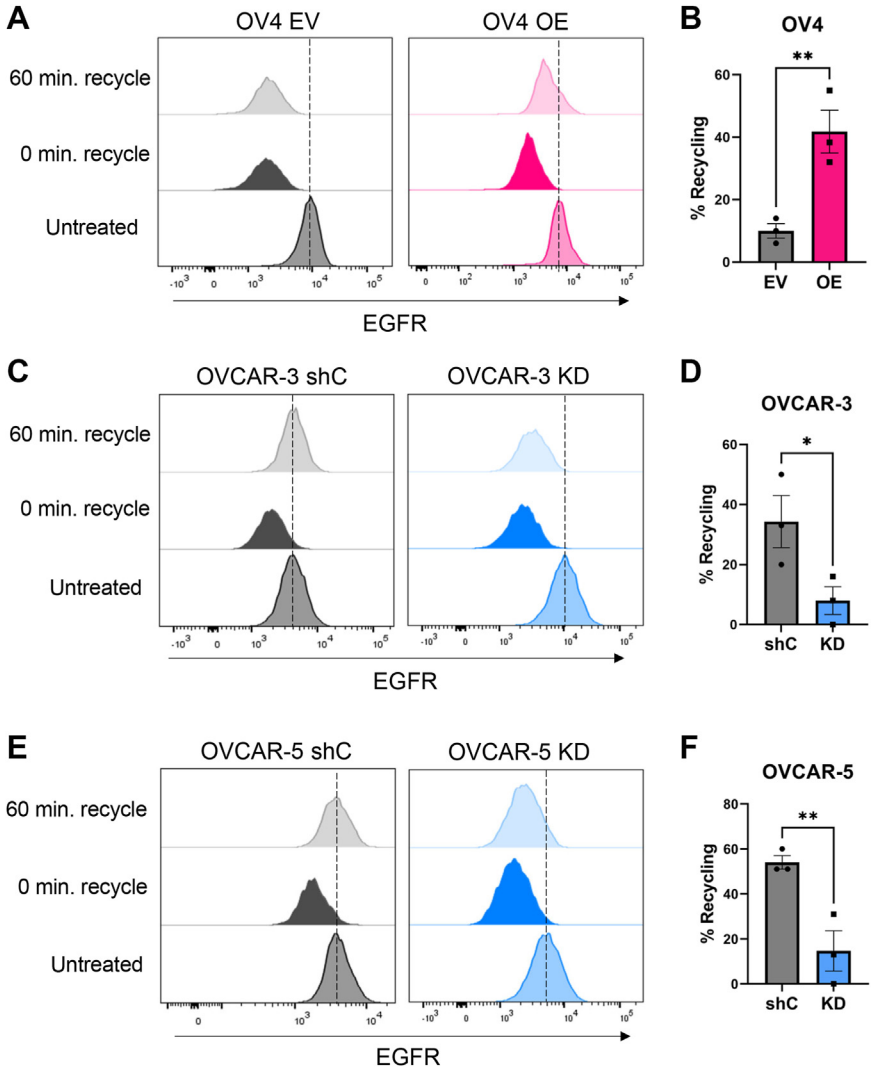

Figure 8. Increased EGFR recycling is observed in cells with high ST6GAL1 expression. Cells were pretreated with 10 μg/ml of CHX to prevent nascent protein synthesis and then treated with 100 ng/ml of EGF for 15 min to induce EGFR internalization. At the end of this incubation, an aliquot of cells was fixed and analyzed for surface EGFR to obtain a baseline measurement immediately after the internalization step, designated as 0 min. The remaining cells were placed in EGF-free media and incubated for another 60 min at 37 °C to allow EGFR recycling. These cells were then fixed and analyzed for surface EGFR. Cells untreated with EGF were used as a control. Percent recycling was calculated by comparing the MFI at 0 min to the MFI at 60 min. *A* and *B*, OV4 cells: representative histogram (*A*) and quantification (*B*) of EGFR recycling. *C* and *D*. OVCAR-3 cells: representative histogram (*C*) and quantification (*D*) of recycling. *E* and *F*, OVCAR-5 cells: representative histogram (*E*) and quantification (*F*) of EGFR recycling. *Dotted lines* indicate the peak MFI of untreated cells. Graphs depict mean and S.D. from three independent experiments. Statistics were calculated using a Student's *t* test (*$p < 0.05$, **$p < 0.01$). CHX, cycloheximide; EGFR, epidermal growth factor receptor; MFI, mean fluorescent intensity.

OV4 OE and EV cells serve as an "on/off" system for ST6GAL1 expression (given that OV4 parental cells have no detectable endogenous ST6GAL1). Total internal reflection fluorescence (TIRF) microscopy was used to assess higher-order clustering of EGFR, which has been proposed to promote EGFR activation and downstream signaling (34). TIRF selectively images within 100 nm of the cell membrane and is therefore a useful method for evaluating membrane protein distribution on the cell surface (35). TIRF was combined with reflection interference contrast microscopy (RICM), a method that detects the cell's contact area with the surface of the coverslip, thus enabling measurements of the spread area of the adhered cell (representative RICM and TIRF images in Fig. 10*A*). RICM analyses showed that a 5-min treatment with EGF stimulated cell spreading, and the cell contact area was larger in EGF-treated OE *versus* EV cells (Fig. 10*B*). TIRF was then used to monitor EGFR clustering, and data were normalized to the cell contact area. Compared with EGF-treated EV cells, EGF-treated OE cells displayed a significant increase in the number (Fig. 10*C*) and size (Fig. 10*D*) of EGFR clusters, as well as an increase in the integrated surface EGFR intensity (Fig. 10*E*). No differences in EGFR clustering were noted in EV and OE cells in the absence of EGF simulation. These data support the hypothesis that α2,6 sialylation enhances EGFR homodimerization and higher-order clustering.

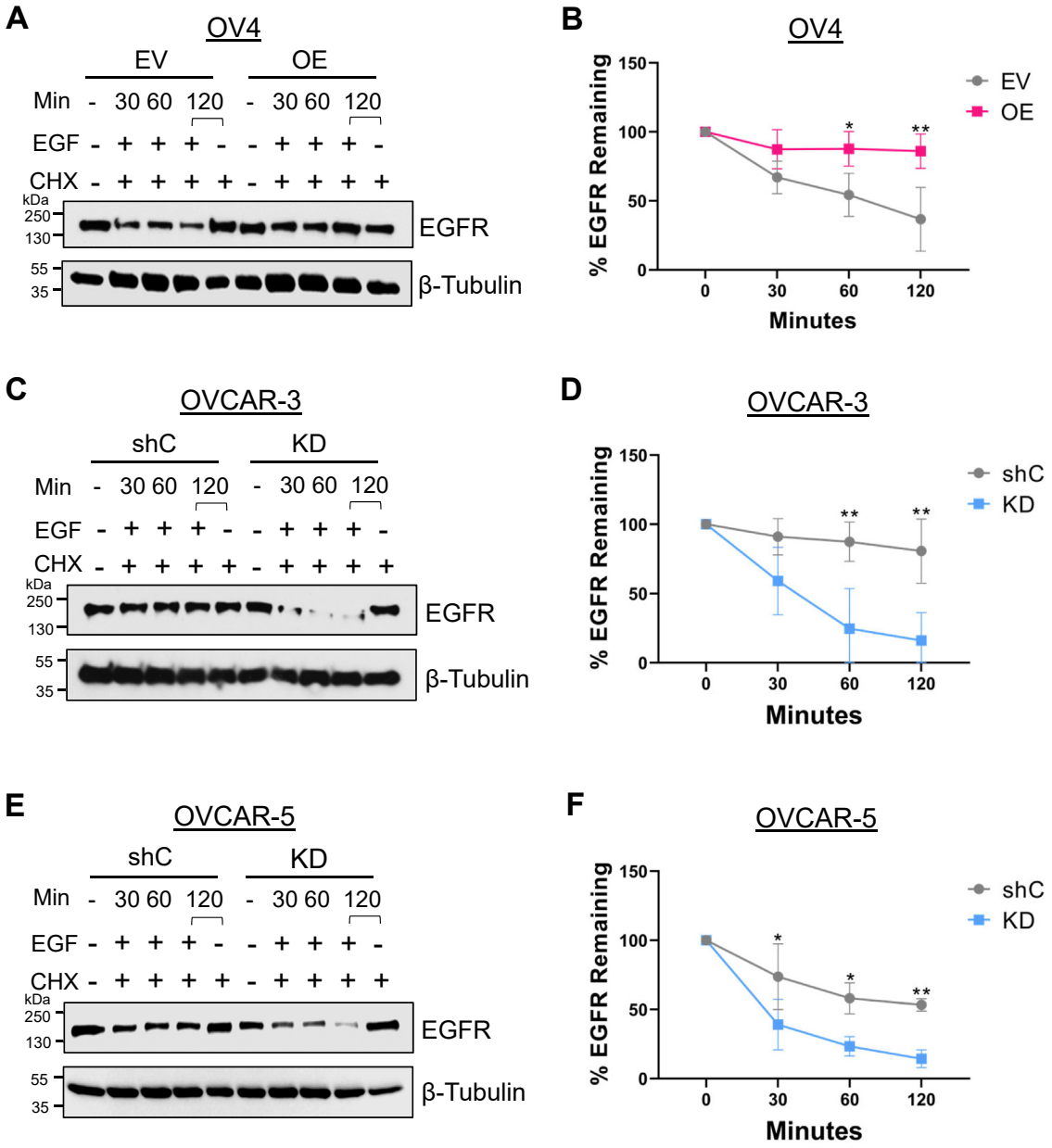

Figure 9. ST6GAL1 activity protects against EGF-induced EGFR degradation. Cells were pretreated with 10 μg/ml of CHX for 2 h to prevent nascent protein synthesis. Cells were then treated with EGF for 30, 60, or 120 min. As controls, cells were left untreated, or treated for 120 min with CHX alone. *A* and *B*, OV4 cells: representative immunoblots (*A*) and quantification (*B*) of the percent EGFR remaining. *C* and *D*, OVCAR-3 cells: representative immunoblots (*C*) and quantification (*D*) of the percent EGFR remaining. *E* and *F*, OVCAR-5 cells: representative immunoblots (*E*) with quantification (*F*) of the percent EGFR remaining. The percent EGFR remaining was calculated by densitometry, comparing values for EGF-stimulated degradation to the CHX control. Graphs depict mean ± S.D. from three independent experiments. Statistics were calculated by using a two-way ANOVA followed by Šidák's multiple comparison test (ns: $p > 0.05$, $^{**}p < 0.01$, $^{***}p < 0.001$, $^{****}p < 0.0001$). CHX, cycloheximide; EGFR, epidermal growth factor receptor.

Upon EGF stimulation, cells with high ST6GAL1 expression have enhanced EGFR colocalization with recycling endosomes and decreased colocalization with lysosomes

To monitor EGFR trafficking throughout the cell, widefield z-stack images were acquired and deconvolved, allowing the generation of 3D reconstructions portraying EGFR localization within distinct subcellular compartments including endosomes and lysosomes. To assess recycling endosomes, cells were treated with EGF for 30 min and then costained for EGFR and Rab11, an established recycling endosomal marker (36). In agreement with the recycling assays shown in Figure 8, we found that EGFR in OV4 OE cells had significantly greater colocalization with Rab11-positive endosomes following EGF treatment as compared with EV cells (representative images in Fig. 11*A*; quantification in Fig. 11*B*). To assess lysosomal colocalization, we treated cells with EGF for 60 min and costained cells for EGFR and the lysosomal marker, LAMP1 (37). In this case, OE cells had reduced colocalization of EGFR and LAMP1 compared with EV cells, suggesting decreased trafficking to the lysosome (representative images in Figure 12*A*; quantification in Fig. 12*B*). Lysosomal-mediated degradation is the predominant mechanism by which EGFR is degraded (7);

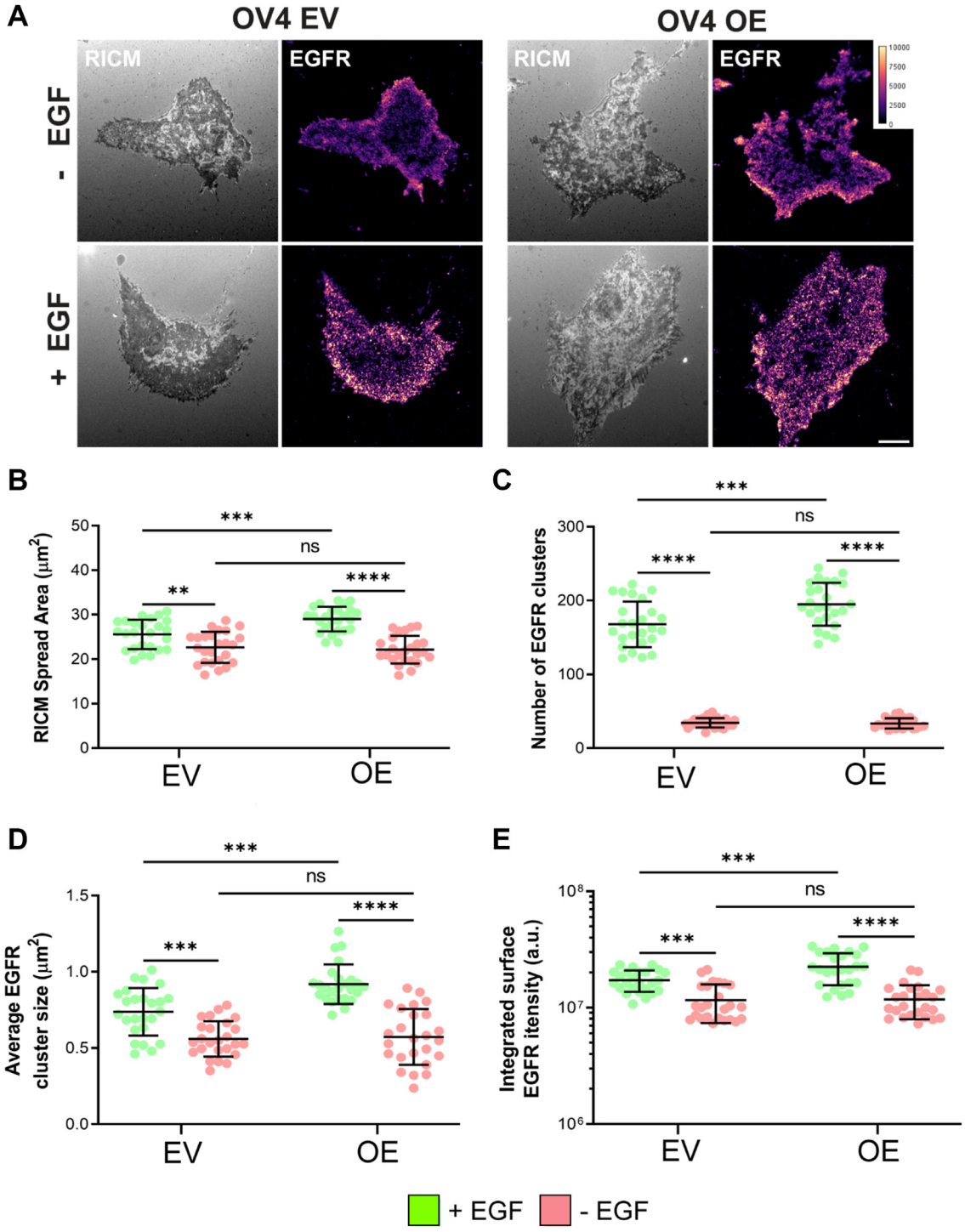

Figure 10. Cells with high ST6GAL1 expression display enhanced higher order clustering of EGFR. *A*, OV4 EV and OE cells were treated with or without EGF for 5 min and stained for EGFR. Representative images are shown for cells visualized by RICM (*grayscale*) or TIRF. Images depict EGFR distributed on the plasma membrane, scale bar = 10 μm. The color key represents the range of pixel intensity values in arbitrary units (a.u.). For all of the images analyzed, pixel values fell within the indicated range. *B*, RICM data showing the spread area of the cell. *C–E*, TIRF results (normalized to the area of the cell as measured by RICM) with quantification of: the number of EGFR clusters per cell (*C*); the average EGFR cluster size (μm^2) (D); and the integrated surface EGFR intensity (*E*). Graphs depict mean ± S.D. from two independent experiments with 25 cells analyzed per experiment. Data were analyzed by ANOVA with Tukey's test, ns: $p > 0.05$, $^{**}p < 0.01$, $^{***}p < 0.001$, $^{****}p < 0.0001$. EGFR, epidermal growth factor receptor; RICM, reflection interference contrast microscopy; TIRF, total internal reflection fluorescence.

therefore, these data align with results in Figure 9 showing enhanced EGFR degradation in cells lacking ST6GAL1. Taken together, these data suggest that the α2,6 sialylation of EGFR acts as a switch to divert EGFR trafficking to recycling endosomes, thus promoting EGFR surface localization and downstream signaling.

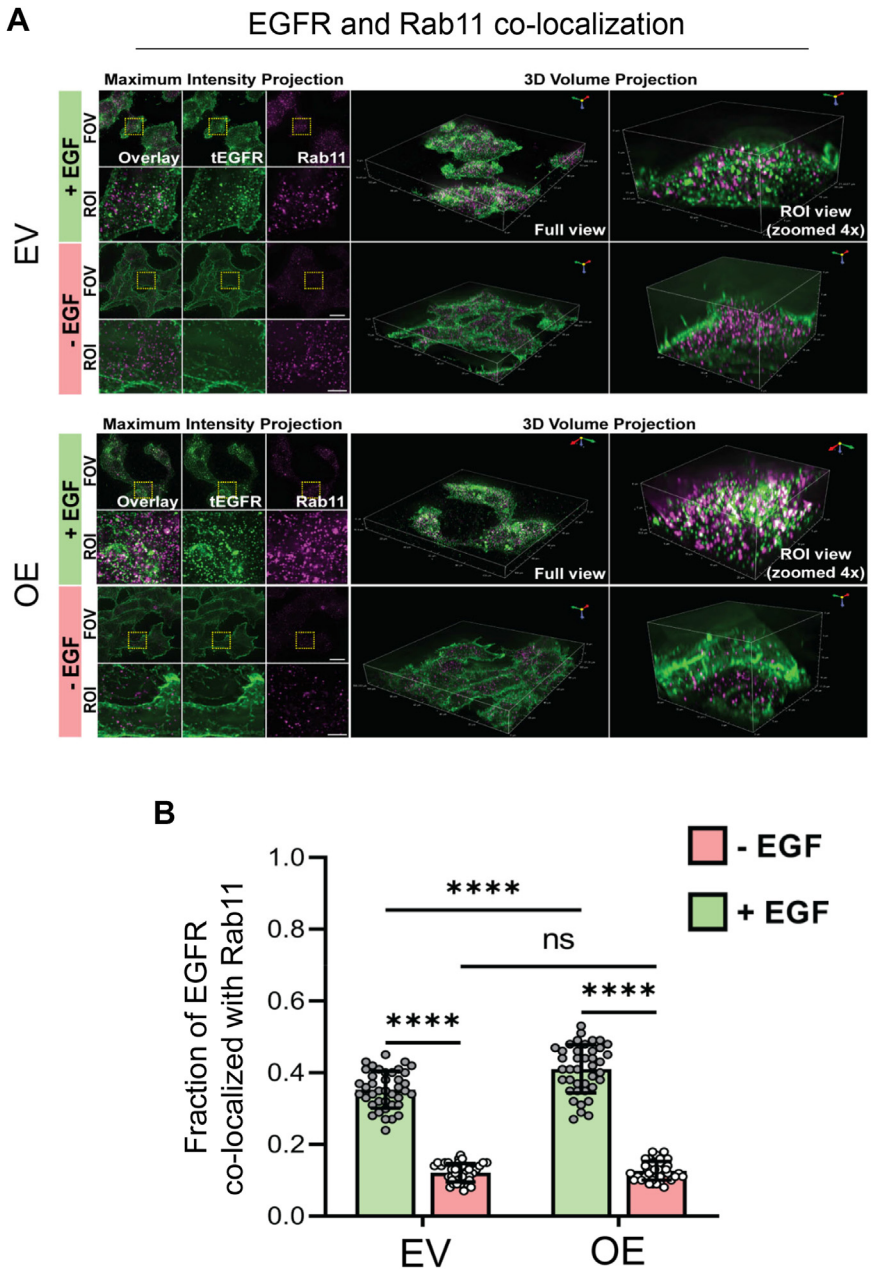

Figure 11. Increased EGFR association with Rab11-positive recycling endosomes is observed in cells expressing ST6GAL1. *A*, maximum intensity projection and 3D volume projection images for OV4 EV and OE cells treated with or without EGF for 30 min. Images were obtained using 3D widefield-deconvolution microscopy. The images depict the EGFR (*green*) and Rab11 (*magenta*) distribution obtained following the processing of the acquired widefield 3D Z-stack images by the Richardson-Lucy algorithm for deconvolution. Scale bar for the field of view (FOV) = 20 μm, region of interest (ROI) = 5 μm. *B*, quantification of the fraction of EGFR colocalized with Rab11-positive endosomes was executed using the JACoP plugin in Fiji. Graphs depict mean ± S.D. from two independent experiments with 40 cells analyzed per group. Data were analyzed by one way ANOVA with Tukey's test (ns: $p > 0.05$, ****$p < 0.0001$). EGFR, epidermal growth factor receptor; JACoP, Just Another Colocalization Plugin; OE, overexpressed.

Discussion

Alterations in glycosylation have long been associated with cancer (38, 39); however, compared with other areas of cancer research, cancer glycobiology remains greatly understudied. One of the predominant glycan changes in a cancer cell is an increase in α2,6-linked sialic acids on N-glycans, which occurs, in part, as a consequence of ST6GAL1 upregulation (18–21). ST6GAL1-mediated sialylation imparts protumorigenic properties by modulating the structure and function of select cell surface receptors (20, 40). For instance, ST6GAL1-mediated sialylation of the TNFR1 and Fas death receptors prevents ligand-induced apoptosis by hindering receptor internalization (41–44), an event required for caspase activation. Additionally, α2,6 sialylation of CD45 and platelet endothelial cell adhesion molecule (PECAM) modulates receptor oligomerization (45, 46), whereas α2,6 sialylation of the β1 integrin promotes cell migration and invasion (47–49). Finally, we and others have identified EGFR as a target for ST6GAL1-mediated sialylation (22–27). However, the mechanisms by which α2,6

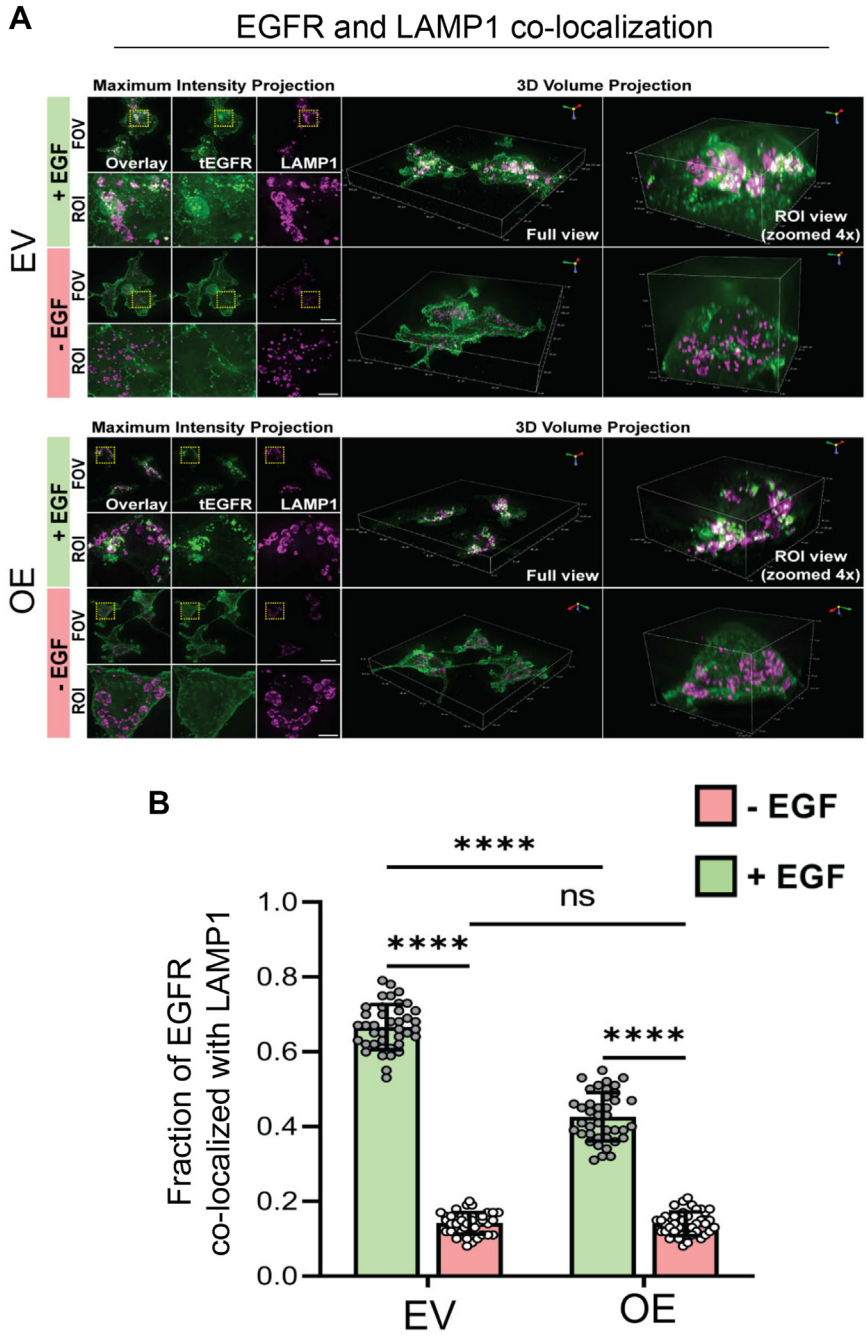

Figure 12. Decreased EGFR localization with lysosomes is observed in cells expressing ST6GAL1. *A*, maximum intensity projection and 3D volume projection images for OV4 EV and OE cells treated with or without EGF for 60 min. Cells were visualized by 3D widefield-deconvolution microscopy. The images depict the EGFR (*green*) and LAMP1 (*magenta*) distribution obtained following the processing of the acquired widefield 3D Z-stack images by the Richardson-Lucy algorithm for deconvolution. Scale bar for the field of view (FOV) = 20 μm, region of interest (ROI) = 5 μm. *B*, quantification of the fraction of EGFR colocalized with LAMP1-positive lysosomes was executed using the JACoP plugin in Fiji. Graphs depict mean ± S.D. from two independent experiments with 40 cells analyzed per group. Data were analyzed by one way ANOVA with Tukey's test (ns: $p > 0.05$, ****$p < 0.0001$). EGFR, epidermal growth factor receptor; JACoP, Just Another Colocalization Plugin; OE, overexpressed.

sialylation modulates EGFR activation and downstream signaling were previously unclear.

In the present study, we examined EGFR activation in cells with ST6GAL1 KD or OE, or in cells with high or low surface α2,6 sialylation as indicated by SNA staining. Across these various models, high ST6GAL1 expression and α2,6 sialylation consistently correlated with the activation of EGFR. Liu *et al.* described similar results in T-cell acute lymphoblastic leukemia cells, finding that ST6GAL1 KD diminished, and ST6GAL1 OE promoted, EGFR signaling (25). Other groups, however, have reported an inhibitory effect of sialylation on EGFR (26–29). Wong's group showed that treatment of cancer cells with a sialidase enzyme caused an increase in EGFR activation, which was attributed to enhanced EGFR clustering (28, 29). However, the sialidase utilized in these studies cleaves all of the major sialic acid linkages (α2,3, α2,6, and α2,8). The

broad ablation of sialoglycans from the cell surface is not biologically equivalent to selectively eliminating the α2,6 sialylation on N-glycans (18). In addition to Wong's work, Park *et al.* (27) and Rodrigues *et al.* (26) reported a negative correlation between ST6GAL1 activity and EGFR activation. The reasons underlying the contradictory results regarding the effects of EGFR sialylation are not currently understood. One factor worth noting is that the SW48 cell line was used as a model in many prior studies that suggested an inhibitory effect of α2,6 sialylation (26, 27). SW48 cells harbor a G719S mutation in EGFR, which has been shown to promote ligand-independent activation of the receptor (30). Nonetheless, in our studies, the overexpression of ST6GAL1 in SW48 cells enhanced EGF-induced EGFR activation, consistent with our other cell models. While additional research will be needed to address the discrepant results regarding ST6GAL1's effects on EGFR, we find that ST6GAL1 activity activates EGFR in the seven cell models studied herein, in addition to four other cell models described in our prior publications (22–24). Moreover, EGFR is markedly activated in the acinar cells of transgenic mice with forced expression of ST6GAL1 in the pancreas (50).

Our studies further suggest that the ST6GAL1-mediated sialylation of EGFR promotes formation of the active EGFR homodimer, as well as higher-order clustering of EGFR. Other investigators have assessed the effects of global sialylation on EGFR dimer formation and clustering (28, 29, 51); however, our results highlight a critical function for a specific sialic acid linkage, mediated by a unique sialyltransferase, in regulating EGFR dimerization and oligomerization. In addition, we demonstrate that α2,6 sialylation modulates the trafficking and fate of EGFR following EGF-induced receptor internalization. Results from recycling assays and 3D Z-stack imaging indicate that sialylation of EGFR by ST6GAL1 promotes its recycling and association with Rab11-positive recycling endosomes. Correspondingly, α2,6 sialylation of EGFR inhibits its degradation and association with LAMP1-positive lysosomes. Prior studies have reported that glycosylation modulates EGFR degradation (52–54); however, the effect of ST6GAL1-mediated sialylation on EGFR degradation was previously unexplored. Likewise, this is the first report demonstrating a role for α2,6 sialylation in EGFR trafficking, to our knowledge.

It is well-known that the glycosylation of EGFR plays a pivotal part in regulating its structure. For example, the N-glycan on Asn-579 is critical for the formation of the autoinhibitory tether. Ablation of this N-glycan weakens the tether, enabling the assembly of preformed dimers in the absence of ligand (17). Reis' group reported that the Asn-579 N-glycan is, in fact, sialylated in cells with ST6GAL1 overexpression (Asn-579 is listed as Asn-603 in this reference due to the inclusion of the signal peptide in amino acid numbering) (26). It is tempting to speculate that the addition of the bulky, negatively charged sialic acid to the Asn-579 N-glycan might interfere with formation of the autoinhibitory tether, promoting EGFR activation. Like the Asn-579 glycosite, an N-glycan on Asn-420 helps to maintain an inactive EGFR conformation. Deletion of the Asn-420 N-glycan promotes spontaneous oligomer formation and constitutive EGFR activation (55). In other studies, molecular dynamics simulations have indicated that N-glycans form noncovalent interactions with amino acids in the EGFR extracellular domain, which, in turn, stabilize the EGF binding site (15). Finally, the N-glycosylation of EGFR contributes to the orientation of the EGFR ectodomain (16). In particular, the EGFR N-glycans adjacent to the plasma membrane help propel the ligand binding domains I and III away from the membrane, thereby, facilitating EGF binding. These various investigations underscore the importance of N-glycans in regulating EGFR structure and activation; however, the specific role of sialylation in these processes remains undetermined.

Beyond modulating EGFR signaling, it has been reported that the α2,6 sialylation of EGFR promotes resistance to various types of EGFR-targeted therapies such as the TKI gefitinib, and the monoclonal antibody, cetuximab (23, 26, 27). Hence, it is essential to understand the mechanisms by which sialylation of EGFR regulates its structure and function. The current investigation shows that ST6GAL1-mediated sialylation of EGFR promotes receptor dimerization, clustering and recycling, thereby slowing EGFR degradation and promoting prosurvival signaling through AKT and NFκB. EGFR recycling, as well as signaling by AKT and NFκB, play well-known roles in fostering resistance to radiotherapy and also targeted therapies including antibodies and TKIs (56–58). Our collective results provide novel insights into the functional consequences of EGFR sialylation in regulating its activation, signaling networks, and trafficking dynamics in malignant cells.

Experimental procedures

Cell culture

MiaPaCa-2, OVCAR-3, and OVCAR-5 cells were obtained from the American Type Culture Collection. S2-013 cells were donated by Dr Michael Hollingsworth at the University of Nebraska. OV4 cells were obtained from Dr Timothy Eberlein at Harvard University. S2-LM7AA cells were donated by Dr Donald Buchsbaum at the University of Alabama at Birmingham. Cells were grown in Dulbecco's modified Eagle's medium (DMEM) (MiaPaCa-2), RPMI-1640 (OVCAR-3, OVCAR-5, Suit-2, S2-013, S2-LM7AA), Leibovitz-L15 (SW48) or DMEM/F12 (OV4) supplemented with 1% antibiotic/antimycotic supplements (Gibco, 15240–062). OVCAR-3 cells were supplemented with 20% fetal bovine serum (FBS) and 0.01 mg/ml of bovine insulin (Sigma-Aldrich, I0516) and all other cells were supplemented with 10% FBS. All cell lines were grown in 5% CO_2 except for the SW48 line, which was grown in 0% CO_2. SW48 and OV4 cells were transduced with lentivirus encoding an EV (Sigma-Aldrich) or the human ST6GAL1 gene (OE) (Genecopoeia). OVCAR-3, OVCAR-5, S2-013, S2-LM7AA cells were transduced with lentivirus containing a shRNA control sequence targeting GFP (shC) (Sigma-Aldrich) or shRNA against ST6GAL1 (KD) (Sigma-Aldrich, TRCN00000035432, sequence: CCGGCGTGTGC TACTACTACCAGAACTCGAGTTCTGGTAGTAGTAGCA CACGTTTTTG). MiaPaCa-2 cells were transduced with an EV lentivirus or the above sequence for shRNA against the ST6GAL1 gene (KD). Lentiviral transductions were performed

using an MOI of 5 and stable polyclonal populations were selected using puromycin (5 μg/ml). Modulation of ST6GAL1 expression was confirmed by SNA staining and immunoblotting. For EGF treatments, cells were serum-deprived for 2 h using media with 1% FBS. A total of 100 ng/ml of EGF (R&D Systems, 236-EG-01M) was then added in 1% FBS containing media for the indicated time intervals.

Immunoblotting

Cells were treated with or without EGF followed by lysis in radioimmunoprecipitation assay buffer (RIPA) (Pierce, 89901) supplemented with protease and phosphatase inhibitors (Pierce, 78440). Total protein concentration was confirmed by bicinchoninic acid assay (Pierce, 23225). Proteins were resolved by SDS-PAGE, and transferred to a polyvinylidene difluoride membrane (Millipore, IPVH00010). Membranes were blocked in 5% nonfat dry milk in Tris-buffered saline containing 0.1% Tween-20 (TBS-T). Membranes were then probed with antibodies for EGFR (1:1000, Cell Signaling Technologies, 4267), p-EGFR (1:1000, pTyr1068, Cell Signaling Technologies, 3777), AKT (1:1000, Cell Signaling Technologies, 4691), p-AKT (1:1000, pSer473, Cell Signaling Technologies, 4060), NFκB p65 (1:1000, Cell Signaling Technologies, 8242), p-NFκB p65 (1:500, pSer536, Cell Signaling Technologies, 3033), ERK1/2 (1:1000, Cell Signaling Technologies, 4695) and p-ERK1/2 (1:1000, p-Thr202/p-Tyr204, Cell Signaling Technologies, 4377). Blots were washed and incubated in horseradish peroxidase-conjugated anti-rabbit secondary antibodies (1:2500, Cell Signaling Technologies, 7074). Equal protein loading was confirmed using β-tubulin (1:2500, Abcam, ab21058 and 1:1000, Invitrogen, MA5-16308). Blots were developed with ECL Western Blotting Substrate (Pierce, 32106), Clarity Western ECL Substrate (Bio-Rad, 1705061), or SuperSignal West Femto (Pierce, 34096). Blots are representative of at least three independent experiments. Densitometry was measured in Fiji (ImageJ, National Institute of Health), and the phosphoproteins were normalized to their respective total protein to obtain a relative densitometry value which was then normalized to β-tubulin. All statistics were calculated in GraphPad Prism (Version 9.5.1, https://www.graphpad.com) using a two-way ANOVA followed by Šidák's multiple comparison test. All results are shown as the mean ± the standard deviation (SD).

Flow cytometry

Adherent cells were detached with accutase (BioLegend, 423201) and blocked on ice with 1% bovine serum albumin (BSA) in PBS. Cells were washed with 0.01% BSA in PBS and incubated with their corresponding antibodies for 30 min on ice. For total EGFR staining, cells were stained with 10 μg/ml of EGFR-Alexa Fluor 488 Clone AY13 (Biolegend, 352908). For SNA staining, cells were incubated with 20 μg/ml of SNA-FITC (Vector, FL-1301–2). For p-EGFR/SNA costaining, cells were treated with EGF for 10 min as described under "Cell culture". After treatment with EGF, cells were washed, fixed in 3.7% paraformaldehyde (PFA) (Electron Microscopy Services, 15710), permeabilized in 0.003% (*v/v*) Triton X-100, washed in PBS and stained with p-EGFR (p-Tyr1068) antibody (Cell Signaling Technologies, 3777) at a 1:1000 dilution and 20 μg/ml of SNA. Cells were washed in PBS and anti-rabbit Alexa Fluor 488 (Invitrogen, A-11034) was added at 4 μg/ml. After staining, cells were washed and evaluated on the LSRII flow cytometer (BD Biosciences). Data were analyzed using FlowJo version 8 software (https://www.flowjo.com) (BD Biosciences) to obtain the MFI. For p-EGFR/SNA analysis, the 10% of cells with the highest levels of SNA staining were designated as "SNA high", and the 10% of cells with the lowest levels of SNA staining were denoted as "SNA low". Levels of p-EGFR staining were then measured in these populations. Statistics were performed using GraphPad Prism. A two-way ANOVA was used followed by Šidák's multiple comparison test. Results shown represent the MFIs ± SD

SNA lectin precipitation

Five hundred micrograms of cell lysate were incubated with 150 μg of SNA-agarose on a rotator at 4 °C overnight (Vector Labs, AL-1303). Proteins containing α2,6 sialic acid were then precipitated by centrifugation and washed 3 times with ice-cold PBS. Precipitates were immunoblotted for EGFR as described above.

Ligand binding assay

Cells were detached using accutase and blocked in 1% BSA on ice as previously described. Cells were then incubated with serial dilutions ranging from 200 nM to 0.39 nM of biotin-conjugated EGF (Invitrogen, E3477) in 0.01% BSA for 1 h on ice. The cells were washed with PBS and incubated in 1 μg/ml of streptavidin conjugated to Alexa Fluor 488 (Invitrogen, S11223) in 0.01% BSA for 30 min. Cells were analyzed *via* flow cytometry as previously described. To obtain the fraction of maximum staining, the MFI at each concentration was divided by the MFI at the highest concentration of EGF. Values were plotted against the log of the concentration used. Graphs represent the mean ± SD from three independent experiments. Data were graphed in GraphPad Prism.

BS^3 cross-linking

The cross-linking protocol was adapted from Turk *et al.* 2015 (32). Cells were treated with EGF at 37 °C for the indicated times and then immediately placed on ice. Cells were washed with ice-cold PBS and BS^3 (Pierce, PG82083) was added to a final concentration of 3 mM. Cells were incubated with BS^3 on ice for 20 min and then the reaction was quenched with 250 mM glycine for 5 min. Cells were washed with PBS and then lysed. Lysates were immunoblotted for EGFR as above. Densitometry was employed to evaluate levels of the EGFR dimer and monomer, and data were reported as the dimer to monomer ratio. Data shown are from three independent experiments.

Recycling assay

Cells were incubated in 10 μg/ml of CHX (Sigma-Aldrich, C7698) for 2 h at 37 °C and then placed on ice for 5 min.

Media containing 1% FBS, 10 μg/ml CHX, and 100 ng/ml of EGF were subsequently added and cells were incubated for 15 min on ice to allow EGF to bind EGFR. Cells were switched to 37 °C for 15 min to enable internalization of the EGF/EGFR complexes. Following this incubation, an aliquot of cells was fixed in PFA and stained for EGFR to obtain a baseline measurement of the amount of EGFR remaining on the surface after the internalization step (designated as "time 0" for the recycling assay). For the remaining cells, EGF-containing media were replaced with EGF-free media containing 1% FBS and 10 μg/ml CHX and cells were incubated at 37 °C for 60 min to allow receptor recycling. Cells were subsequently detached with accutase and fixed in 3.7% PFA. EGFR staining was performed as above. Percent recycling was calculated by subtracting the MFI at time 0 from the MFI obtained at 60 min. This value was then divided by the MFI at 60 min and multiplied by 100 to obtain a percentage value. Statistics were calculated in GraphPad Prism using a Student's *t* test. Results are shown as the mean ± SD.

Degradation assay

Cells were incubated in media containing 1% FBS and 10 μg/ml CHX for 2 h. EGF was then added to the cells as previously described and incubated for 30, 60, or 120 min. Cells were lysed and immunoblotted for EGFR. As controls, cells were either left untreated, or treated with CHX alone for 120 min. Densitometric values were calculated using ImageJ and normalized to β-tubulin. The percent EGFR remaining was calculated by comparing normalized densitometric values to the CHX control. Statistics were performed using GraphPad Prism using a two-way ANOVA followed by Šidák's multiple comparison test. Data are plotted as the mean ± SD.

RICM and TIRF microscopy

OV4 EV and OE cells were seeded overnight on glass coverslips (Thorlabs, CG15XH) coated with fibronectin (Sigma-Aldrich, F1141). Cells were serum-starved (1% FBS) for 2 h and then treated with EGF for 5 min as described under "Cell culture". Cells were fixed using 3.7% formaldehyde (Electron Microscopy Services, 15710) for 10 min at 37 °C. Cells were washed with PBS five times, permeabilized, and blocked with 0.25% Triton X-100 and 1% BSA for 30 min. Cells were stained for 2 h at 37 °C with primary antibody against EGFR (1:50, Invitrogen, MA5-13269). Cells were then washed five times in PBS and incubated for 1 h in secondary anti-mouse Alexa Fluor 488 (1:250, Invitrogen, A32766) at 37 °C. After washing in PBS, cells were imaged in FluoroBrite DMEM (Gibco, A1896701). To evaluate surface EGFR distribution and clustering, TIRF and RICM were conducted as previously described (59). Briefly, OV4 cells were imaged on a Nikon Eclipse Ti2 microscope using the Nikon Elements software with an oil immersion Apo TIRF 60 × NA 1.49 objective and an ORCA-Flash 4.0 V3 Digital CMOS camera (Hamamatsu). The sample was illuminated with a Sola epifluorescence light source (Lumencor) for RICM or with 488 nm laser for TIRF.

3D widefield microscopy

OV4 EV and OE cells were seeded overnight on glass coverslips coated with fibronectin as described above. For Rab11 imaging, cells were treated with EGF for 30 min and for LAMP1 imaging, cells were treated with EGF for 60 min. Cells were fixed and blocked as described under RICM and TIRF microscopy. Cells were stained for EGFR (1:50, Invitrogen, MA5-13269), Rab11 (1:50, Cell Signaling, 5589), or LAMP1 (1:100, Cell Signaling, 9091) for 2 h at 37 °C. Cells were then washed and incubated for 1 h at 37 °C with anti-rabbit Alexa Fluor 647 (1:250, Invitrogen, A32733) or anti-mouse Alexa Fluor 488 (1:250, Invitrogen, A32766). Cells were washed in PBS and imaged in FluoroBrite DMEM (Gibco, A1896701). To obtain widefield Z-stacks, cells were imaged on a Nikon Eclipse Ti2 microscope using Nikon Elements software with a 100 nm step size in the Z dimension. Images were acquired with a 470/40 excitation filter and a 525/50 emission filter for Alexa Fluor 488 or a 620/60 excitation filter and a 700/75 emission filter for Alexa Fluor 647.

Image processing and analysis

Custom-written ImageJ macros were employed to subtract background fluorescence and measure morphological parameters, including the area of the cell footprint (RICM area), integrated intensity, and size and number of EGFR clusters. The RICM image was outlined manually to define the cell boundary and calculate the cell area. Integrated EGFR intensity was determined by subtracting the background measured from an off-cell region and then calculating the total fluorescence intensity within the cell boundary. The number and size analyses for EGFR clusters were estimated using the analyze particle function in Fiji following default thresholding of the background-subtracted image to generate a mask. The widefield Z-stack images were deconvolved using Nikon Elements deconvolution software (Richardson Lucy; parameters: 50 iterations, low noise level). Colocalization analysis was performed using the Fiji (ImageJ, National Institute of Health) plugin JACoP (Just Another Colocalization Plugin) to quantify Mander's correlation coefficients (60). Statistical analysis by one-way ANOVA was performed using GraphPad Prism. All results are presented as mean ± SD.

Data availability

All data described in this study are contained within the manuscript.

Acknowledgments—The authors would like to thank Dr Jihye Hwang for technical assistance and the UAB Comprehensive Flow Cytometry Core.

Author contributions—K. E. A., T. C. R., A. L. M., and S. L. B. conceptualization; K. E. A., T. C. R., A. L. M., and S. L. B. methodology; K. E. A., T. C. R., A. L. M., and S. L. B. investigation; K. E. A., T. C. R., A. L. M., and S. L. B. visualization; K. E. A., and T. C. R. formal analysis; K. E. A., and T. C. R. data curation; K. E. A. writing– original draft; K. E. A., T. C. R., A. L. M., and S. L. B. writing– review

and editing; T. C. R. and A. L. M. software; A. L. M. and S. L. B. project administration; A. L. M. and S. L. B. funding acquisition.

Funding and additional information—These studies were supported by grants from the National Institutes of Health (U01 CA233581 and R01 CA225177) and the UAB O'Neal Comprehensive Cancer Center (O'Neal Invests) to S. L. B. The work was also supported by grants from the National Science Foundation (CAREER 1832100) and the O'Neal Comprehensive Cancer Center (O'Neal Invests) to A. L. M. and K. E. A. was supported by the T32 Training Program in Cell, Molecular and Developmental Biology (T32 GM008111). The Comprehensive Flow Cytometry Core was supported by grants from the National Institutes of Health to the Center for AIDS Research (AI027767) and the O'Neal Comprehensive Cancer Center (CA013148). The content in this manuscript is solely the responsibility of the authors and does not necessary represent the official view of the National Institutes of Health.

Conflict of interest—The authors declare that they have no conflicts of interest with the contents of this article.

Abbreviations—The abbreviations used are: CHX, cycloheximide; DMEM, Dulbecco's modified Eagle's medium; EGFR, epidermal growth factor receptor; EV, empty vector; KD, knocked-down; MFI, mean fluorescent intensity; OE, overexpressed; PFA, paraformaldehyde; p-EGFR, phosphorylated EGFR; RICM, reflection interference contrast microscopy; SNA, Sambucus nigra agglutinin; TIRF, total internal reflection fluorescence; TKI, tyrosine kinase inhibitor.

References

1. Schlessinger, J. (2014) Receptor tyrosine kinases: legacy of the first two decades. *Cold Spring Harb. Perspect. Biol.* **6**. https://doi.org/10.1101/cshperspect.a008912
2. Chen, J., Zeng, F., Forrester, S. J., Eguchi, S., Zhang, M.-Z., and Harris, R. C. (2016) Expression and function of the epidermal growth factor receptor in physiology and disease. *Physiol. Rev.* **96**, 1025–1069
3. Wee, P., and Wang, Z. (2017) Epidermal growth factor receptor cell proliferation signaling pathways. *Cancers* **9**, 52
4. Yarden, Y., and Pines, G. (2012) The ERBB network: at last, cancer therapy meets systems biology. *Nat. Rev. Cancer* **12**, 553–563
5. Gan, H. K., Cvrljevic, A. N., and Johns, T. G. (2013) The epidermal growth factor receptor variant III (EGFRvIII): where wild things are altered. *FEBS J.* **280**, 5350–5370
6. Ray, P., Tan, Y. S., Somnay, V., Mehta, R., Sitto, M., Ahsan, A., *et al.* (2016) Differential protein stability of EGFR mutants determines responsiveness to tyrosine kinase inhibitors. *Oncotarget* **7**, 68597–68613
7. Sigismund, S., Avanzato, D., and Lanzetti, L. (2018) Emerging functions of the EGFR in cancer. *Mol. Oncol.* **12**, 3–20
8. Shostak, K., and Chariot, A. (2015) EGFR and NF-κB: partners in cancer. *Trends Mol. Med.* **21**, 385–393
9. Lemmon, M. A., and Schlessinger, J. (2010) Cell signaling by receptor tyrosine kinases. *Cell* **141**, 1117–1134
10. Tomas, A., Futter, C. E., and Eden, E. R. (2014) EGF receptor trafficking: consequences for signaling and cancer. *Trends Cell Biol.* **24**, 26–34
11. Freed, D. M., Bessman, N. J., Kiyatkin, A., Salazar-Cavazos, E., Byrne, P. O., Moore, J. O., *et al.* (2017) EGFR ligands differentially stabilize receptor dimers to specify signaling kinetics. *Cell* **171**, 683–695.e618
12. Gomes Ferreira, I., Pucci, M., Venturi, G., Malagolini, N., Chiricolo, M., and Dall'Olio, F. (2018) Glycosylation as a main regulator of growth and death factor receptors signaling. *Int. J. Mol. Sci.* **19**, 580
13. Zhen, Y., Caprioli, R. M., and Staros, J. V. (2003) Characterization of glycosylation sites of the epidermal growth factor receptor. *Biochemistry* **42**, 5478–5492
14. Takahashi, M., Hasegawa, Y., Maeda, K., Kitano, M., and Taniguchi, N. (2022) Role of glycosyltransferases in carcinogenesis; growth factor signaling and EMT/MET programs. *Glycoconj J.* **39**, 167–176
15. Azimzadeh Irani, M., Kannan, S., and Verma, C. (2017) Role of N-glycosylation in EGFR ectodomain ligand binding. *Proteins* **85**, 1529–1549
16. Kaszuba, K., Grzybek, M., Orłowski, A., Danne, R., Róg, T., Simons, K., *et al.* (2015) N-Glycosylation as determinant of epidermal growth factor receptor conformation in membranes. *Proc. Natl. Acad. Sci. U. S. A.* **112**, 4334–4339
17. Whitson, K. B., Whitson, S. R., Red-Brewer, M. L., McCoy, A. J., Vitali, A. A., Walker, F., *et al.* (2005) Functional effects of glycosylation at Asn-579 of the epidermal growth factor receptor. *Biochemistry* **44**, 14920–14931
18. Schultz, M. J., Swindall, A. F., and Bellis, S. L. (2012) Regulation of the metastatic cell phenotype by sialylated glycans. *Cancer Metast. Rev.* **31**, 501–518
19. Dorsett, K. A., Marciel, M. P., Hwang, J., Ankenbauer, K. E., Bhalerao, N., and Bellis, S. L. (2020) Regulation of ST6GAL1 sialyltransferase expression in cancer cells. *Glycobiology* **31**, 530–539
20. Garnham, R., Scott, E., Livermore, K. E., and Munkley, J. (2019) ST6GAL1: a key player in cancer. *Oncol. Lett.* **18**, 983–989
21. Lu, J., and Gu, J. (2015) Significance of β-galactoside α2,6 sialyltranferase 1 in cancers. *Molecules* **20**, 7509–7527
22. Britain, C. M., Bhalerao, N., Silva, A. D., Chakraborty, A., Buchsbaum, D. J., Crowley, M. R., *et al.* (2021) Glycosyltransferase ST6Gal-I promotes the epithelial to mesenchymal transition in pancreatic cancer cells. *J. Biol. Chem.* **296**, 100034
23. Britain, C. M., Holdbrooks, A. T., Anderson, J. C., Willey, C. D., and Bellis, S. L. (2018) Sialylation of EGFR by the ST6Gal-I sialyltransferase promotes EGFR activation and resistance to gefitinib-mediated cell death. *J. Ovarian Res.* **11**. https://doi.org/10.1186/s13048-018-0385-0
24. Rao, T. C., Beggs, R. R., Ankenbauer, K. E., Hwang, J., Ma, V. P., Salaita, K., *et al.* (2022) ST6Gal-I-mediated sialylation of the epidermal growth factor receptor modulates cell mechanics and enhances invasion. *J. Biol. Chem.* **298**, 101726
25. Liu, Q., Ma, H., Sun, X., Liu, B., Xiao, Y., Pan, S., *et al.* (2019) The regulatory ZFAS1/miR-150/ST6GAL1 crosstalk modulates sialylation of EGFR *via* PI3K/Akt pathway in T-cell acute lymphoblastic leukemia. *J. Exp. Clin. Cancer Res.* **38**, 199
26. Rodrigues, J. G., Duarte, H. O., Gomes, C., Balmaña, M., Martins Á, M., Hensbergen, P. J., *et al.* (2021) Terminal α2,6-sialylation of epidermal growth factor receptor modulates antibody therapy response of colorectal cancer cells. *Cell Oncol. (Dordr)* **44**, 835–850
27. Park, J. J., Yi, J. Y., Jin, Y. B., Lee, Y. J., Lee, J. S., Lee, Y. S., *et al.* (2012) Sialylation of epidermal growth factor receptor regulates receptor activity and chemosensitivity to gefitinib in colon cancer cells. *Biochem. Pharmacol.* **83**, 849–857
28. Liu, Y. C., Yen, H. Y., Chen, C. Y., Chen, C. H., Cheng, P. F., Juan, Y. H., *et al.* (2011) Sialylation and fucosylation of epidermal growth factor receptor suppress its dimerization and activation in lung cancer cells. *Proc. Natl. Acad. Sci. U. S. A.* **108**, 11332–11337
29. Yen, H. Y., Liu, Y. C., Chen, N. Y., Tsai, C. F., Wang, Y. T., Chen, Y. J., *et al.* (2015) Effect of sialylation on EGFR phosphorylation and resistance to tyrosine kinase inhibition. *Proc. Natl. Acad. Sci. U. S. A.* **112**, 6955–6960
30. Ito, K., Nishio, M., Kato, M., Murakami, H., Aoyagi, Y., Ohe, Y., *et al.* (2019) TAS-121, A selective mutant EGFR inhibitor, shows activity against tumors expressing various EGFR mutations including T790M and uncommon mutations G719X. *Mol. Cancer Ther.* **18**, 920–928
31. Yachida, N., Yoshihara, K., Suda, K., Nakaoka, H., Ueda, H., Sugino, K., *et al.* (2021) Biological significance of KRAS mutant allele expression in ovarian endometriosis. *Cancer Sci.* **112**, 2020–2032
32. Turk, H. F., and Chapkin, R. S. (2015) Analysis of epidermal growth factor receptor dimerization by BS^3 cross-linking. *Methods Mol. Biol.* **1233**, 25–34
33. Schneider-Poetsch, T., Ju, J., Eyler, D. E., Dang, Y., Bhat, S., Merrick, W. C., *et al.* (2010) Inhibition of eukaryotic translation elongation by cycloheximide and lactimidomycin. *Nat. Chem. Biol.* **6**, 209–217

34. Huang, Y., Bharill, S., Karandur, D., Peterson, S. M., Marita, M., Shi, X., *et al.* (2016) Molecular basis for multimerization in the activation of the epidermal growth factor receptor. *eLife* **5**, e14107
35. Mattheyses, A. L., Simon, S. M., and Rappoport, J. Z. (2010) Imaging with total internal reflection fluorescence microscopy for the cell biologist. *J. Cell Sci.* **123**, 3621–3628
36. Ullrich, O., Reinsch, S., Urbé, S., Zerial, M., and Parton, R. G. (1996) Rab11 regulates recycling through the pericentriolar recycling endosome. *J. Cell Biol.* **135**, 913–924
37. Medina, D. L., Fraldi, A., Bouche, V., Annunziata, F., Mansueto, G., Spampanato, C., *et al.* (2011) Transcriptional activation of lysosomal exocytosis promotes cellular clearance. *Dev. Cell* **21**, 421–430
38. Pinho, S. S., and Reis, C. A. (2015) Glycosylation in cancer: mechanisms and clinical implications. *Nat. Rev. Cancer* **15**, 540–555
39. Bellis, S. L., Reis, C. A., Varki, A., Kannagi, R., and Stanley, P. (2022) Glycosylation changes in cancer. In: Varki, A., Cummings, R. D., Esko, J. D., Stanley, P., Hart, G. W., Aebi, M., *et al.* eds. *Essentials of Glycobiology, Chapter 47*, 4th edition, Cold Spring Harbor Laboratory Press, Cold Spring Harbor, New York. https://doi.org/10.1101/glycobiology.4e.47
40. Gc, S., Bellis, S. L., and Hjelmeland, A. B. (2022) ST6Gal1: oncogenic signaling pathways and targets. *Front. Mol. Biosci.* **9**, 962908
41. Swindall, A. F., and Bellis, S. L. (2011) Sialylation of the Fas death receptor by ST6Gal-I provides protection against Fas-mediated apoptosis in colon carcinoma cells. *J. Biol. Chem.* **286**, 22982–22990
42. Holdbrooks, A. T., Britain, C. M., and Bellis, S. L. (2018) ST6Gal-I sialyltransferase promotes tumor necrosis factor (TNF)-mediated cancer cell survival *via* sialylation of the TNF receptor 1 (TNFR1) death receptor. *J. Biol. Chem.* **293**, 1610–1622
43. Liu, Z., Swindall, A. F., Kesterson, R. A., Schoeb, T. R., Bullard, D. C., and Bellis, S. L. (2011) ST6Gal-I regulates macrophage apoptosis *via* α2-6 sialylation of the TNFR1 death receptor. *J. Biol. Chem.* **286**, 39654–39662
44. Alexander, K. L., Serrano, C. A., Chakraborty, A., Nearing, M., Council, L. N., Riquelme, A., *et al.* (2020) Modulation of glycosyltransferase ST6Gal-I in gastric cancer-derived organoids disrupts homeostatic epithelial cell turnover. *J. Biol. Chem.* **295**, 14153–14163
45. Kitazume, S., Imamaki, R., Ogawa, K., Komi, Y., Futakawa, S., Kojima, S., *et al.* (2010) Alpha2,6-sialic acid on platelet endothelial cell adhesion molecule (PECAM) regulates its homophilic interactions and downstream antiapoptotic signaling. *J. Biol. Chem.* **285**, 6515–6521
46. Amano, M., Galvan, M., He, J., and Baum, L. G. (2003) The ST6Gal I sialyltransferase selectively modifies N-glycans on CD45 to negatively regulate galectin-1-induced CD45 clustering, phosphatase modulation, and T cell death. *J. Biol. Chem.* **278**, 7469–7475
47. Christie, D. R., Shaikh, F. M., Lucas, J. A., 4th, Lucas, J. A., 3rd, and Bellis, S. L. (2008) ST6Gal-I expression in ovarian cancer cells promotes an invasive phenotype by altering integrin glycosylation and function. *J. Ovarian Res.* **1**. https://doi.org/10.1186/1757-2215-1-3
48. Shaikh, F. M., Seales, E. C., Clem, W. C., Hennessy, K. M., Zhuo, Y., and Bellis, S. L. (2008) Tumor cell migration and invasion are regulated by expression of variant integrin glycoforms. *Exp. Cell Res.* **314**, 2941–2950
49. Seales, E. C., Shaikh, F. M., Woodard-Grice, A. V., Aggarwal, P., McBrayer, A. C., Hennessy, K. M., *et al.* (2005) A protein kinase C/Ras/ERK signaling pathway activates myeloid fibronectin receptors by altering beta1 integrin sialylation. *J. Biol. Chem.* **280**, 37610–37615
50. Bhalerao, N., Chakraborty, A., Marciel, M. P., Hwang, J., Britain, C. M., Silva, A. D., *et al.* (2023) ST6GAL1 sialyltransferase promotes acinar to ductal metaplasia and pancreatic cancer progression. *JCI Insight*. e161563. https://doi.org/10.1172/jci.insight.161563
51. Leong, S. K., Hsiao, J. C., and Shie, J. J. (2022) A multiscale molecular dynamic analysis reveals the effect of sialylation on EGFR clustering in a CRISPR/Cas9-Derived model. *Int. J. Mol. Sci.* **23**. https://doi.org/10.3390/ijms23158754
52. Wu, L., Cheng, Y., Geng, D., Fan, Z., Lin, B., Zhu, Q., *et al.* (2022) O-GlcNAcylation regulates epidermal growth factor receptor intracellular trafficking and signaling. *Proc. Natl. Acad. Sci. U. S. A.* **119**, e2107453119
53. Lin, W. L., Lin, Y. S., Shi, G. Y., Chang, C.-F., and Wu, H. L. (2015) Lewisy promotes migration of oral cancer cells by glycosylation of epidermal growth factor receptor. *PLoS One* **10**, e0120162
54. Arriagada, C., Cavieres, V. A., Luchsinger, C., González, A. E., Muñoz, V. C., Cancino, J., *et al.* (2020) GOLPH3 regulates EGFR in T98G glioblastoma cells by modulating its glycosylation and ubiquitylation. *Int. J. Mol. Sci.* **21**, 8880
55. Tsuda, T., Ikeda, Y., and Taniguchi, N. (2000) The Asn-420-linked sugar chain in human epidermal growth factor receptor suppresses ligand-independent spontaneous oligomerization. Possible role of a specific sugar chain in controllable receptor activation. *J. Biol. Chem.* **275**, 21988–21994
56. Blakely, C. M., Pazarentzos, E., Olivas, V., Asthana, S., Yan, J. J., Tan, I., *et al.* (2015) NF-κB-activating complex engaged in response to EGFR oncogene inhibition drives tumor cell survival and residual disease in lung cancer. *Cell Rep.* **11**, 98–110
57. Zhang, L., Xie, B., Qiu, Y., Jing, D., Zhang, J., Duan, Y., *et al.* (2020) Rab25-Mediated EGFR recycling causes tumor acquired radioresistance. *iScience* **23**, 100997
58. Jacobsen, K., Bertran-Alamillo, J., Molina, M. A., Teixidó, C., Karachaliou, N., Pedersen, M. H., *et al.* (2017) Convergent Akt activation drives acquired EGFR inhibitor resistance in lung cancer. *Nat. Commun.* **8**, 410
59. Rao, T. C., and Mattheyses, A. L. (2022) Tension gauge tether Probes for quantifying growth factor mediated integrin mechanics and adhesion. *JoVE*. https://doi.org/10.3791/63529
60. Bolte, S., and Cordelières, F. P. (2006) A guided tour into subcellular colocalization analysis in light microscopy. *J. Microsc.* **224**, 213–232